# Journal Pre-proof

Measuring Directed Functional Connectivity Using Non-Parametric Directionality Analysis: Validation and Comparison with Non-Parametric Granger Causality

Timothy O. West, David M. Halliday, Steven L. Bressler, Simon F. Farmer, Vladimir Litvak
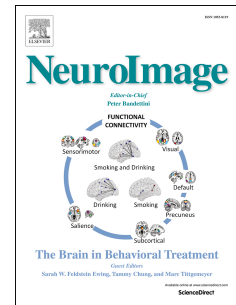
Please cite this article as: West, T.O, Halliday, D.M., Bressler, S.L., Farmer, S.F., Litvak, V., Measuring Directed Functional Connectivity Using Non-Parametric Directionality Analysis: Validation and Comparison with Non-Parametric Granger Causality, *NeuroImage*, https://doi.org/10.1016/j.neuroimage.2020.116796.

This is a PDF file of an article that has undergone enhancements after acceptance, such as the addition of a cover page and metadata, and formatting for readability, but it is not yet the definitive version of record. This version will undergo additional copyediting, typesetting and review before it is published in its final form, but we are providing this version to give early visibility of the article. Please note that, during the production process, errors may be discovered which could affect the content, and all legal disclaimers that apply to the journal pertain.

**Timothy West:** Conceptualization, Methodology, Software, Writing- Original draft preparation, Writing - Review & Editing. **David Hallliday**: Methodology, Software, Writing - Review & Editing. **Steven Bressler:** Conceptualization, Supervision, Writing - Review & Editing. **Simon Farmer:** Conceptualization, Supervision, Writing- Original draft preparation, Writing - Review & Editing. **Vladimir Litvak:** Conceptualization, Resources, Supervision, Writing- Original draft preparation, Writing - Review & Editing.

West et al. (2018): A Novel Non-Parametric Directionality Measure **v5.3**

Journal Pre-proof

# Measuring Directed Functional Connectivity Using Non-Parametric Directionality Analysis: Validation and Comparison with Non-Parametric Granger Causality

Timothy O. West[1,2], David M. Halliday[3], Steven L. Bressler[4], Simon F. Farmer[5,6], and Vladimir Litvak[2]

[1]*Centre for Mathematics and Physics in the Life Sciences and Experimental Biology, UCL Department of Physics and Astronomy, Gower Street, London, WC1E 6BT, UK.*

[2]*Wellcome Centre for Human Neuroimaging, UCL Queen Square Institute of Neurology, London, WC1N 3AR, UK.*

[3]*Department of Electronic Engineering and York Biomedical Research Institute, University of York, YO10 5DD, UK*

[4]*Centre for Complex Systems and Brain Sciences, Florida Atlantic University, 777 Glades Road, Florida, USA.*

[5]*Department of Neurology, National Hospital for Neurology & Neurosurgery, Queen Square, London WC1N 3BG, UK.*

[6]*Department of Clinical and Movement Neurosciences, Institute of Neurology, UCL, London, WC1N 3BG, UK.*

*\*Corresponding Author (timothy.west.10@ucl.ac.uk)*

West et al. (2018): A Novel Non-Parametric Directionality Measure **v5.3**

Journal Pre-proof

# Abstract

21

22 **Background:** 'Non-parametric directionality' (NPD) is a novel method for estimation of directed

23 functional connectivity (dFC) in neural data. The method has previously been verified in its ability to

24 recover causal interactions in simulated spiking networks in Halliday et al. (2015).

25 **Methods:** This work presents a validation of NPD in continuous neural recordings (e.g. local field

26 potentials). Specifically, we use autoregressive models to simulate time delayed correlations between

27 neural signals. We then test for the accurate recovery of networks in the face of several confounds

28 typically encountered in empirical data. We examine the effects of NPD under varying: a) signal-to-

29 noise ratios, b) asymmetries in signal strength, c) instantaneous mixing, d) common drive, e) data

30 length, and f) parallel/convergent signal routing. We also apply NPD to data from a patient who

31 underwent simultaneous magnetoencephalography and deep brain recording.

32 **Results:** We demonstrate that NPD can accurately recover directed functional connectivity from

33 simulations with known patterns of connectivity. The performance of the NPD measure is compared

34 with non-parametric estimators of Granger causality (NPG), a well-established methodology for

35 model-free estimation of dFC. A series of simulations investigating synthetically imposed confounds

36 demonstrate that NPD provides estimates of connectivity that are equivalent to NPG, albeit with an

37 increased sensitivity to data length. However, we provide evidence that: i) NPD is less sensitive than

38 NPG to degradation by noise; ii) NPD is more robust to the generation of false positive identification

39 of connectivity resulting from SNR asymmetries; iii) NPD is more robust to corruption via moderate

40 amounts of instantaneous signal mixing.

41 **Conclusions:** The results in this paper highlight that to be practically applied to neural data,

42 connectivity metrics should not only be accurate in their recovery of causal networks but also resistant

43 to the confounding effects often encountered in experimental recordings of multimodal data. Taken

44 together, these findings position NPD at the state-of-the-art with respect to the estimation of directed

45 functional connectivity in neuroimaging.

# Highlights

46

47 • Non-parametric directionality (NPD) is a novel directed connectivity measure.

48 • NPD estimates are equivalent to estimates of Granger causality but are more robust to signal

49 confounds.

50 • Multivariate extensions of NPD can correctly identify signal routing.

## Keywords

functional connectivity; directionality; EEG; MEG; signal-to-noise; volume conduction; neural networks; computational neuroscience; multimodal data; local field potentials.

## Abbreviations

dFC – Directed functional connectivity

EEG – Electroencephalogram

LFP – Local field potential

MEG – Magnetoencephalogram

MVAR – Multivariate autoregressive (model)

NPD – Non-parametric directionality

(mv) NPG – (multivariate) Non-parametric estimator of Granger causality

SMA – Supplementary motor area

SNR – Signal-to-noise ratio

STN – Subthalamic Nucleus

## 1 Introduction

Questions regarding the causal relationships between anatomically connected regions of the brain have become of fundamental importance across many domains of neuroscience (Sporns 2010; Swanson 2012). A novel method for estimating directed functional connectivity (dFC), termed non-parametric directionality (NPD), has been recently described in Halliday (2015). This method has been demonstrated to yield physiological insights into the connectivity of the cortico-basal-ganglia network when applied to (continuous) field recordings made in rodents (West et al. 2018). In this work we evaluate NPD's performance at recovering known patterns of connectivity in the face of several confounding factors and compare it with another popularly used measure – the estimation of Granger causality.

Functional connectivity is based on a description of the statistical dependencies between different neural signals and is typically estimated through time or frequency domain correlations (Bastos and Schoffelen 2016; Friston 2011). Magnitude squared coherence, equivalent to a frequency domain coefficient of correlation, has been widely adopted as the estimator of choice for functional

79  connectivity in the neuroimaging community (Brillinger 1975; Halliday et al. 1995). Undirected

80  measures of functional connectivity (such as coherence) are symmetrical, giving no indication of the

81  temporal precedence of correlations, a property understood to be a necessary result of causation in

82  time evolving systems (Wiener 1956), nor the predictability of one time series from that of the other.

83  dFC aims to estimate statistical asymmetries in the correlated activity of a set of signals in order to

84  infer the causal influence (or predictability) of one signal over another. Similar to the role played by

85  coherence in measuring undirected functional connectivity, Wiener-Granger causality has emerged as

86  a first-choice estimator of directed connectivity due to its well established theoretical basis (Bressler

87  and Seth 2011; Ding et al. 2006) and its successful application to questions concerning causal

88  networks inferred from large-scale neural recordings (e.g. Brovelli et al. 2004; Richter et al. 2018).

89  Estimates of dFC are most frequently computed in the literature using methods estimating Granger

90  causality (Dhamala et al. 2008a; Geweke 1982; Granger 1969; Kamiński et al. 2001). Granger

91  causality is expressed in terms of the capacity of the information in the past of one signal, *X*, to predict

92  the future of another signal, *Y*. Granger (1969) introduced a straightforward method of estimation

93  through the comparison of an autoregressive model by which the explained variance of *Y* is compared

94  between that of a 'full' model (i.e. accounting for the past of *X* and *Y*) with that of a restricted model

95  (i.e. *Y* only). If a prediction of the future of *Y* is aided by information from the past of *X*, then *X* is said

96  to 'Granger-cause' *Y*. The method requires factoring out the autoregressive component of the signal

97  (i.e. the 'restricted' model) to avoid trivial correlations that occur simply due to the periodicity in the

98  signals.

99  Efforts to estimate Granger causality without resorting to autoregressive models have resulted in an

100 extension of the method termed non-parametric Granger causality (NPG), which avoids the estimation

101 of transfer functions from multivariate autoregressive (MVAR) coefficients (Dhamala et al. 2008a). In

102 NPG, transfer functions and noise covariances are estimated through the spectral factorization of

103 (non-parametrically derived) Fourier coefficients rather from MVAR model parameters. Here, we

104 directly compare NPG with NPD as an estimator of dFC. Both methods share the property of being

105 non-parametric (model-free) approaches which can be derived from identical spectral transforms

106 made either via Fourier or wavelet techniques.

107 NPD is founded on the same principles of causality as Granger, namely that temporally lagged

108 *dependencies* indicate causal direction. NPD works by decomposing the coherence into three

109 temporally independent components separated by the relative lag of the dependencies between the

110 signals: 1) forward lagged; 2) reverse lagged; and 3) instantaneously correlated. Rather than using a

111 naïve cross-correlation estimator that is susceptible to spurious peaks resulting from the individual

112 signals' autocorrelations, NPD takes an approach akin to the factoring out of a 'restricted' model (i.e.

113 of *Y* only) used in Granger. This is achieved through a process of spectral pre-whitening which acts to

114  bring the individual signal's spectra closer to white-noise but preserves the correlations between them.
115  In the original paper (Halliday 2015), the method was validated using a simple three node network
116  with each node's dynamics simulated using a conductance model of a spiking neurone in order to
117  generate a series of discrete point processes. The authors demonstrated that NPD was successful in
118  recovering the connectivity from a range of simulated architectures. Furthermore, the method was
119  applied to spike timings (a point process) recorded from muscle spindle and shown to yield
120  physiologically plausible estimations of causality. Our recent work has extended the application of
121  NPD to continuous local field potential (LFP) recordings made from an *in vivo* preparation of the
122  cortico-basal ganglia system (West et al. 2018).

123  Estimation of empirical dFC in continuous neural recordings such as the LFP or
124  magneto/electroencephalogram (M/EEG) is complicated by a number of factors. These include: low
125  and possibly unequal signal-to-noise ratios (SNRs), instantaneous volume conduction, common drive,
126  signal routing via parallel but disjoint paths, and the presence of cyclic paths within a network. All
127  pose potential confounds for the metrics described here. The failure of Granger causality estimators in
128  the presence of large amounts of measurement noise is a well-established shortcoming (Newbold
129  1978) which becomes particularly acute in noisy electrophysiological recordings (Nalatore et al.
130  2007). Differences in the recording gain between signals is also known to confound estimation of
131  Granger causality, with the most commonly used estimator demonstrating bias towards favouring the
132  strongest signal as the driver (Bastos and Schoffelen 2016; Haufe et al. 2012). This property is likely
133  to be a nuisance when investigating causation between multimodal signal sets such as in experiments
134  involving simultaneous measurements of MEG and LFP where significant differences in recording
135  gain are to be expected (Litvak et al. 2011).

136  Instantaneous mixing of the electromagnetic signals generated by distinct sources in the brain has
137  long been known to make estimation of functional connectivity based on recordings such as the EEG
138  difficult (Haufe et al. 2012; Nunez et al. 1997; Srinivasan et al. 2007). Common presynaptic drive
139  produces correlations in pairs of output spike trains (Farmer et al. 1993), and in pairs of evoked
140  potentials (Truccolo et al. 2002). This problem can lead to spurious estimates of directed connectivity
141  if delays in the arrival of the common input induce lagged correlations between unconnected neurons
142  or neuronal populations. When the common presynaptic input is measured, extensions of functional
143  connectivity metrics built upon partial regressions (so called *conditioned* or *partialized* estimates) can
144  be used to remove common input effects and, subsequently, remove the possibility of spurious
145  inference of directed connectivity between neurones in receipt of lagged common input. Partial
146  regression can be used with both NPD and NPG to reduce the influence of common drive. In the case
147  of NPD, the authors introduced a multivariate extension that can be used to reduce the influence of
148  common drive through partial regression of a third reference signal (Halliday et al. 2016). This
149  method relies upon the reference signal substantially encapsulating the activity of the common drive.

150    In the case that the recordings are incomplete representations of the propagating neural activity, the
151    conditioning will only be partially effective. NPD and NPG conditioned on a third signal can also be
152    used to infer connectivity patterns where two signals are correlated through interaction with an
153    intermediary signal (West et al. 2018).

154    Statistical aspects of coherence estimation have been widely studied. Carter et al. (1973a) highlight
155    that a coherence estimate constructed from averaging over $n$ independent segments has an asymptotic
156    standard deviation proportional to $n^{-0.5}$, suggesting that a large number of segments are required to
157    obtain reliable estimates. Carter et al. (1973b) suggest a reasonable range for $n$ is 32 to 64 segments.
158    The directional decomposition in NPD is based on the use of time lag in a correlation or partial
159    correlation function. As the number of lags is related to the segment length, using shorter segments
160    may impact on the reliability of directional estimates as fewer time lags are available to infer
161    directional information.

162    In this paper we will assess the performance of NPD's ability to recover the connectomes from
163    several simulated architectures and in the presence of the previously stated confounds. We compare
164    the accuracy of connectivity estimation with NPD and NPG under these different conditions.
165    Furthermore, we also test the efficacy of a multivariate extension of NPD, the conditioned NPD, as a
166    means of testing for the effects of common drive and its ability to discriminate between parallel signal
167    routing. The amount of data required for accurate estimation of connectivity will also be assessed.
168    Finally, we bring the presented methods to the analysis of empirically recorded data from patients
169    with Parkinson's disease. Using an example recording, we examine how artificially imposed changes
170    in the signals' SNR and linear mixing can change the estimate of dFC made between signals recorded
171    from the human cortex and basal-ganglia. Our primary goal is to verify the utility of the proposed
172    measure in application to real-world neuroimaging data.

# 173    2    Methods

## 174    2.1    Approach

175    In this study we utilize spectral coherence for estimates of undirected FC, and NPD/NPG for
176    estimates of dFC. We set up models of continuous neural signals with known connectivity
177    architectures parameterized in MVAR coefficients. Confounds such as signal-to-noise and
178    instantaneous mixing are then introduced following simulation of the MVAR process using an
179    observation model. The analyses presented here start with the assumption that any exploratory
180    analyses of the data are complete, including any artefact rejection and/or preprocessing and that one
181    or more significant coherence estimates have been identified as a prerequisite for directional
182    decomposition using NPD. Using coherence, we first establish the existence of coherent frequencies

183    within the modelled data sets. Patterns of connectivity in the models are then recovered using the two

184    dFC metrics (NPD and NPG). As connectivity in the models is known (by design) we analyse how the

185    metrics perform at accurately recovering the known connectivity profiles. Finally, we look at the

186    methods' application to empirical data when used to estimate the directed functional connectivity

187    between the basal ganglia and motor cortex in recordings made from a patient with Parkinson's

188    disease (PD).

## 2.2  Analysis Software and Data Availability

190    Data was analysed using a set of custom scripts written in MATLAB R2017a (The MathWorks,

191    Natick, MA, USA). Non-parametric directionality was implemented using the Neurospec toolbox

192    (http://www.neurospec.org/). MVAR models were implemented using the BSMART toolbox (Cui et

193    al. 2008). NPG calculations and spectral estimates were implemented in FieldTrip (Oostenveld et al.

194    2011b). All scripts for the analyses presented here can be found in a GitHub repository

195    (https://github.com/twestWTCN/NPD_Validate). A full list of script dependencies, toolboxes used,

196    their authors, and links to their original source code can be found in Appendix I. The example patient

197    data used in this paper is anonymised and available upon request.

## 2.3  Functional Connectivity

### 2.3.1  Spectra and Coherence

200    Spectral estimates were made using periodogram estimates utilizing Hanning tapers.    Unless

201    otherwise stated (see section 3.6 in which we investigate the role of data availability), data were

202    divided into segments $2^8$ samples in length (~1.3 s at 200 Hz). We computed the magnitude-squared

203    coherence via:

$$|R_{YX}(\omega)|^2 = \frac{|f_{YX}(\omega)|^2}{f_{XX}(\omega)f_{YY}(\omega)}$$

204                                                                                                    **(1)**

205    where $f_{XX}, f_{YY}, f_{YX}$ are the *X* and *Y* autospectra and *XY* cross-spectrum respectively.

### 2.3.2  Non-Parametric Directionality

207    Non-parametric directionality provides a model-free estimate of directional correlations within a

208    system through the decomposition of the coherence into components separated by their lags yielding

209    separate instantaneous, forward-lagging, and reverse-lagging spectra (Halliday 2015). This is

210    achieved using pre-whitening of the Fourier transforms. This acts to bring the spectral content of a

211    signal closer to that of white noise, in this case using optimal pre-whitening with minimum mean

212    squared error to compute the whitening filter. This procedure is equivalent to generating two new

213    random processes which have spectra equal to 1 at all frequencies:

$$f_{XX}^w(\omega) = 1, f_{YY}^w(\omega) = 1$$

214 **(2)**

215 The prewhitening step effectively eliminates the autocorrelation structure of the respective signals but

216 retains bivariate correlations between them. The pre-whitening brings the denominator of the

217 coherence, the product of the autospectra (a normalization factor) equal to 1. Thus, the coherence can

218 be reduced to the magnitude squared of the minimum mean square error (MMSE) pre-whitened cross

219 spectrum:

220 $$|R_{YX}(\omega)|^2 = f_{YX}^w(\omega).$$

221 **(3)**

222 The overall scalar measure of dependence between $X$ and $Y$, denoted as $R_{YX}^2$, is defined as the integral

223 over the coherence in equation (1). In line with the previous literature, the notation here uses as $R_{YX}^2$ to

224 indicate a scalar measure of overall dependence and $|R_{YX}(\omega)|^2$ to indicate coherence, a function of

225 frequency. As the coherence loses all terms in the denominator, the equivalent cross-spectrum can

226 then be transformed to the time domain to yield the time-domain correlation function:

227 $$\rho_{YX}(\tau) = \frac{1}{2\pi} \int_{-\pi}^{+\pi} f_{YX}^w(\omega) e^{i\omega\tau} d\omega.$$

228 **(4)**

229 This measure can be decomposed (in the time domain) via Parseval's theorem for any desired lag. We

230 choose to separate into reverse, instantaneous, and forward components:

231 $$R_{YX}^2 = \underbrace{\int_{\tau<0}^{0} |\rho_{YX}(\tau)|^2 d\tau}_{X \to Y} + \underbrace{|\rho_{YX}(0)|^2}_{X \leftrightarrow Y} + \underbrace{\int_{0}^{\tau>0} |\rho_{YX}(\tau)|^2 d\tau}_{X \leftarrow Y}.$$

232 **(5)**

233 These components may be abbreviated to:

$$R_{YX}^2 = R_{YX,-}^2 + R_{YX,0}^2 + R_{YX,+}^2$$

234 **(6)**

235 where component $R_{YX,-}^2$ yields correlations in which $Y$ lags $X$, $R_{YX,0}^2$ instantaneous correlations, and

236 $R_{YX,+}^2$ correlations in which $X$ lags $Y$. To create a set of frequency domain measures which decompose

237 coherence into three directional components, the three terms in equation (6) are each Fourier

238 transformed using the lag ranges in equation (5). This creates three frequency domain measures that

239 capture reverse, zero-lag and forward directionality, respectively. Coherence is decomposed by

240 direction using a ratio of the relative magnitude-squared values at each frequency as:

241 $$|R_{YX}(\omega)|^2 = \left|R'_{YX,-}(\omega)\right|^2 + \left|R'_{YX,0}(\omega)\right|^2 + \left|R'_{YX,+}(\omega)\right|^2.$$

242                                                                                                    **(7)**

243    The prime symbol on the RHS of equation (7) is used to indicate that these are not formal coherence

244    measures, but represent one of three directional contributions (reverse, instantaneous and forward) to

245    the coherence. Thus, from each component we can assess spectrally resolved directional interaction

246    whilst accounting for the signals' autocorrelation structure. For a full derivation of the NPD method

247    and details of its algorithmic implementation please refer to Halliday et al. (2016).

### 2.3.3  A Multivariate Extension – Conditioned Non-Parametric Directionality

249    In addition to bivariate NPD, we used a multivariate extension that allows the directional components

250    of coherence to be conditioned upon a third signal (Halliday et al. 2016). The conditionalization of

251    NPD is achieved through a partial regression of $X$ and $Y$ conditioned on $Z$. This analysis decomposes

252    the partial coherence into the same three directional components: forward, reverse, and zero-lag. It

253    can indicate if information in the bivariate interaction shares variance common to signals in other

254    parts of the network. For example, the partial correlation between $X$ and $Y$ with $Z$ as predictor can be

255    used to determine if the flow of information from $X \rightarrow Y$ is independent of area $Z$, or whether the flow

256    of information is $X \rightarrow Z \rightarrow Y$, in which case the partial coherence between $X$ and $Y$ with $Z$ as predictor

257    should be zero. The partial coherence can also be used to investigate if the flow of information is $Z \rightarrow$

258    $X$ and $Z \rightarrow Y$, or if it is $X \rightarrow Y \rightarrow Z$ or $Z \rightarrow X \rightarrow Y$, or in the case of common input $Z \rightarrow X$ *and $Y$*, in

259    which cases the partial coherence, and any directional components, should be zero.

260    The relationship between the squared coherence function $|R_{XY}(\omega)|^2$ and the squared correlation

261    coefficient was the starting point for the derivation of the non-parametric directionality method in

262    Halliday (2015). The correlation coefficient is given by:

$$R_{YX}^2 = \frac{\sigma_Y^2 - \sigma_{Y|X}^2}{\sigma_Y^2}$$

263                                                                                                    **(8)**

264    where the conditioned variance, $\sigma_{Y|X}^2$ is the variance of the error process following a linear regression

265    of Y on X. It then follows that the correlation coefficient may be conditioned to account for any

266    common effect that a process Z may have on both X and Y by also estimating the residuals following

267    regression with Z:

$$R_{YX|Z}^2 = \frac{\sigma_{Y|Z}^2 - \sigma_{Y|X,Z}^2}{\sigma_{Y|Z}^2}$$

268                                                                                                    **(9)**

269    in which the processes X and Y are both conditioned (regressed) against the third process Z. Partial

270    regression is often useful in situations in which it is believed that the tertiary signal Z can account for

271    some or all of the original association between X and Y. Thus, the objective is to distinguish whether

272    there is a genuine correlation $R_{YX}^2$ that is distinct from the apparent one induced by Z: $R_{YX|Z}^2$. In the

273    same manner by which the correlation coefficient may be conditioned to account for any common

274    effect that a process Z may have on both X and Y, we can condition the estimated coherence

275    $|R_{YX}(\omega)|^2$ on Z:

$$|R_{YX|Z}(\omega)|^2 = \frac{|f_{YX|Z}(\omega)|^2}{f_{XX|Z}(\omega)f_{YY|Z}(\omega)}$$

276                                                                                                  **(10)**

277    In this way we can form a so called 'partial' coherence to determine the association of the coherence

278    between X and Y with predictor Z. By using this form of the coherence as the starting step we can

279    continue with the same decomposition as was made before for bivariate NPD, in order to attain an

280    estimate of the NPD between X and Y but conditioned on Z. In practice we achieve conditioning of

281    the respective autospectra $f_{XX|Z}(\omega)$ and $f_{YY|Z}(\omega)$ using the approach set out in Brillinger (1988). This

282    method has been used successfully in LFP recordings to recover known anatomical pathways in the

283    basal-ganglia (West et al. 2018). For full details of the derivation and implementation of conditioned

284    NPD, see Halliday et al. (2016).

285    Increased levels of additive noise can impact on partial coherence estimates but should not distort any

286    temporal precedence present in the triplets of signals (Baccalá and Sameshima 2006). Conditioned

287    NPD uses decomposition by time lag to infer directionality so should be robust to increased levels of

288    additive noise in the predictor. We explore the extent to which this is true in simulations of triadic

289    networks in results section 3.8.

## 2.3.4 Non-Parametric Granger Causality and its Relation to NPD

291    Granger causality is based on the premise that if a signal *X* causes a signal *Y*, then the past values of *X*

292    can be used to predict the state of *Y* beyond that of the information contained in the past of *Y* alone

293    (Granger 1969). This has conventionally been tested in the context of multivariate autoregressive

294    models fit to the data, and in which the explained variance of *Y* via a 'restricted' model based on *Y*

295    alone is compared to that of a 'full' model using information of both the past of *X* and *Y* (Geweke

296    1982). Frequency domain extensions of Granger have been developed (Geweke 1982; Kamiński et al.

297    2001) and applied widely across many domains of neuroscience (e.g. Brovelli et al. 2004).

298    The requirement to fit multiple MVAR models can cause several difficulties in analyses, namely: i)

299    the requirement of large model orders to capture complex spectral features; ii) computational cost of

300    model inversion; and iii) assumptions as to the correlation structure of the data in order to capture the

301    signal as an MVAR process. In order to avoid the requirement for the estimation of MVAR models,

302    Dhamala et al. (2008) proposed a non-parametric estimator of Granger Causality. This estimator can

West et al. (2018): A Novel Non-Parametric Directionality Measure                    **v5.3**

Journal Pre-proof

303    be derived from widely used Fourier or wavelet based spectral estimation methods which do not

304    suffer from these complications. The method hinges on the derivation of a spectral matrix directly

305    from the spectral transforms of the data (i.e. Fourier or wavelet) instead of the full transfer and noise

306    covariance matrices specified in an inverted MVAR model. Subsequently, the spectral matrix is

307    factorized to derive the transfer function and noise covariance matrices of the set of signals (Sayed

308    and Kailath 2001). Via this technique it is possible to decompose the total power spectrum of Y

309    between its intrinsic power and the *causal* contribution from X. The first term refers to the *intrinsic*

310    power of Y, the second term to a causal contribution to the power of Y from X. For a full derivation

311    and details of its implementation please refer to Dhamala et al. (2008).

312    The difference between the way NPG and NPD determine causal or directional components is that

313    NPG uses a decomposition of the signal power into intrinsic and extrinsic components, whereas NPD

314    decomposes a normalised correlation coefficient according to time lag. Both NPG and NPD use a

315    frequency domain approach. The frequency approach in NPG uses the formulation in Geweke (1982)

316    in combination with factorization of the spectral matrix (Wilson, 1972), see Dhamala et al. (2008a,

317    2008b) for details. NPD is based on the approach of Pierce (1979) to decompose the product moment

318    correlation coefficient and coherence summatively into directional components. The starting point is

319    the spectral matrix (as in NPG). The decomposition is achieved by generating an MMSE pre-whitened

320    spectral matrix, $F_w$, as:

321
$$F_w = \begin{pmatrix} 1 & f_{YX}(f_{XX}f_{YY})^{-0.5} \\ f_{XY}(f_{XX}f_{YY})^{-0.5} & 1 \end{pmatrix},$$

322                                                                                                      **(11)**

323    where $f_{YY}$ and $f_{XX}$ are the autospectra, and $f_{YX}$ and $f_{XY}$ are the cross spectra, with frequency argument

324    omitted. The effect of this pre-whitening allows coherence to be calculated directly from the cross-

325    spectra. NPD thus decomposes coherence according to time lag in the normalised correlation whereas

326    NPG decomposes the spectrum into intrinsic and extrinsic factors, the presence of non-zero intrinsic

327    factors is taken as indicative of a causal effect in NPG.

### 2.3.5 Pairwise Versus Multivariate Applications of Metrics

329    Both NPD and NPG can be used in either a bivariate (pairwise) or a full multivariate (i.e. greater than

330    two signals) framework. As pairwise analyses of dFC are by far the most common approach used in

331    the current literature we primarily make a comparison of bivariate NPD and NPG computed between

332    two signals only. However, when investigating issues such as common drive and the influence of

333    tertiary signals we utilize the multivariate extension of NPG (mvNPG; Wen et al. 2013) and compare

334    it with conditioned NPD. mvNPG extends Geweke's formulation of Granger beyond pairwise

335    analyses using spectral matrix factorization. In combination with Dhamala's approach to obtain

336 spectral matrices from Fourier transforms of data this yields a method by which it is possible to create

337 a non-parametric estimator of causality in high dimensional data. mvNPG used here is implemented in

338 Fieldtrip (Oostenveld et al. 2011a).

339 Conditioned NPD is indicated by the use of brackets to signify the conditioning signal (e.g. NPD(x)

340 signifies NPD conditioned on signal X). This approach is used exclusively in section 3.1 (common

341 drive) and 3.8 (incomplete signals for conditioning).

## 2.4 Generation of Synthetic Data

342

### 2.4.1 Multivariate Autoregressive Modelling

343

344 In order to simulate data that models lagged propagation between simple periodic systems we used

345 MVAR modelling. MVAR models are an extension to 1-dimensional autoregressive models in which

346 a model variable can be expressed as a linear combination of its previous values plus some stochastic

347 error term. A $P^{th}$ order MVAR model with $N$ number of states is given by:

$$X_t = c + \sum_{i=1}^{P} A_i X_{t-i} + \epsilon_t$$

348 **(12)**

349 where $X_t$ is a $[N \times 1]$ vector of values at time $t$, and $X_{t-i}$ are the values at time $(t-i)$. $A_1, \dots, A_P$ are

350 $[N \times N]$ matrices of autoregressive coefficients at lag $i$, $c$ is a vector of constants, and $\epsilon_t$ is

351 innovation noise (Gaussian) with zero mean and covariance $R$. An AR model of order $P$ describes the

352 $N$ values at time, $X_t$, as a linear combination of $P$ previous values, $X_{t-i}$, a set of constants, $c$, and a

353 vector of additional noise values, $\varepsilon_t$. The $P$ matrices $A_i$ $(i = 1, \dots, P)$ specify the linear dependencies

354 in the model at time lag $i$. Simple periodic signals may be engineered in the MVAR formulation by

355 setting of alternating signed coefficients at different lags. For example, to obtain a lag two periodicity

356 of the system variable $X$ we set $A_{1,2} = [1 - 1]$. The alternating signs of the coefficients set up the

357 signal to oscillate with a period equal to the difference in lags. In order to introduce correlations

358 between variables we introduced non-zero coefficients off the diagonal. In this way we simulate

359 lagged connectivity by setting positive coefficients between nodes at lags greater than 1. For the

360 parameters of the simulated MVAR models please see appendix II. Simulations were made using the

361 BSMART toolbox. All simulations were run with sample length $T$, where $T = 5$ x $10^4$ data samples

362 (except in sets of simulations investigating data availability and benchmarking; see below). In order to

363 set a time scale of the simulations we chose an arbitrary sampling frequency of 200 Hz which places

364 simulations around the frequencies typically observed in neural data. This yields total simulation time

365 of 250s (unless otherwise stated). The model architecture for each set of figures is outlined using a

366 ball and stick diagram next to the main results. All MVAR models used were tested for asymptotic

367    stability by determining that the absolute value of the eigenvalues of a model's companion matrix

368    were less than 1 (as per Lütkepohl 2005).

### 2.4.2 Observation Modelling

370    To introduce the effects of changes in SNR and instantaneous mixing of signals that can arise due to

371    the practical aspects of experimental recordings of neural signals, we construct an observation model

372    on top of the model of the dynamics that maps from the hidden internal variables $X$ onto the

373    externally observed variables $Y$. This function adds observation noise to the MVAR signal and then

374    applies an instantaneous linear combination of the internal variables:

$$Y = z(LX) + \lambda\gamma$$

375    **(13)**

376    where $Y$ is a vector of observations created using the vector of internal variables, $X$, combined with a

377    vector of additive observation noise (i.i.d, zero-mean, unit-variance, white noise) $\gamma$ weighted by

378    scalar factor $\lambda$ which determines the effective SNR of the observed variables. The function $z(\cdot)$

379    indicates z-standardization to zero mean and unit variance. A $[N \times N]$ mixing matrix $L$ is used to

380    introduce dependencies between the observed signals. There is a constraint on the diagonal of $L$ such

381    that $L_{i=j} = 1, i = 1, ..., N$ such that the gain of the signals themselves was unaltered. Thus, we specify

382    the mixing between signals by specifying the off-diagonal entries of matrix $L$. When applied to z-

383    normalized, uncorrelated data, the mixing matrix introduces shared variance equal to the square-root

384    of the off-diagonal coefficients of $L$ (Halliday et al. 2016).

385    We compute the decibel SNR as the log ratio of signal variances i.e. 1:1 SNR is equivalent to 0 dB. In

386    some simulations we investigate the role of asymmetric SNR and so report the difference of SNRs

387    between signals: $\Delta SNR_{XY} = SNR_{X(dB)} - SNR_{Y(dB)}$. Assuming one signal is held constant then a

388    difference in SNRs of 10 dB is equivalent to 10 times increase in the noise in the other signal, 20 dB

389    equivalent to 100 times increase, etc. SNR calculations are computed from the ratios of the mean

390    narrowband power within the range of the peak frequency of activities ±5 Hz with that of the

391    background noise, providing good coverage over the example signals used here. In empirical

392    neuroimaging data where multiple origins of noise exist, this is a much harder quantity to estimate

393    (Parkkonen 2010). We however use +12 dB as the level for the weakest signal, equivalent to a good

394    quality EEG recording (Goldenholz et al. 2009).

## 2.5 Benchmarking the Metrics: Data Length, Number of Connections, and Combined Confounders

397    To determine the quantity of data required to use either NPD or NPG for the accurate estimation of

398    dFC, we setup a benchmark test and then examine how the score of this benchmark changes with the

399 amount of available data and number of connections in a given network. We also use this benchmark

400 to assess how a combination of confounding effects can influence network estimation. First, we

401 randomly simulate three sets of 24 random directed graphs with a fixed number of vertices ($n = 3$)

402 including either one, two, or three edges in total. These graphs are then simulated as MVAR models

403 (as detailed above) by placing non-zero autoregressive coefficients with a random lag uniformly

404 distributed in the interval [1 3]. The simulated data is then analysed with NPD and NPG. By using a

405 non-parametric permutation test to form confidence intervals (see section 2.7.1 below) for each

406 measure we determine the detection of a directed connection if 10% of the spectra for the given pair

407 of nodes is over the 99.99% confidence limit to yield a predicted adjacency matrix $\hat{M}$. For every

408 element of $\hat{M}$ that is equal to that in the actual adjacency matrix $M$ (i.e. a true positive or negative) the

409 score is +1; for every non-equal element (i.e. false positive or negative) the score is -1. Thus, the

410 maximum score in a three-node network is +6 (all correct) and the minimum is -6. We report scores as

411 percentages of the maximum from -100% to 100%.

412 In the first set of benchmarks we investigate both the role of data availability and the number of

413 connections in a graph. We perform the benchmark with the 24 random graphs using: i) a fixed

414 amount of data (500s), but variable trial length ($2^3$ to $2^{10}$) (such as is the case when deciding how to

415 epoch data from a 'steady-state'); and ii) a variable amount of data but a fixed number of trials (n =

416 100) (such is the case when analysing an event related study with a set number of repetitions).

417 In the second set of benchmarks we investigate how the combination of asymmetric SNR and signal

418 mixing effects act to confound connectivity estimation. We make a 12 x 12 design, adding noise to the

419 target node to achieve a range of narrowband (50-60 Hz) $\Delta SNR_{1,2}$ of -45 dB to 0 dB and then adding

420 signal mixing to achieve 0% to 100% shared variance. The weakest signal is again clamped to 12 dB.

421 Note that the adjustment of SNR is done before signal mixing. The benchmark is then applied for data

422 simulated from the 24 random graphs described above.

## 2.6 Experimental Data

### 2.6.1 Experimental Protocol

425 In the final experiment of this paper, we investigate how the two dFC metrics (NPD and NPG)

426 perform when estimating the dFC between the cerebral cortex (supplementary motor area; SMA) and

427 the subthalamic nucleus (STN). This connection has been reported to be predominantly cortically

428 leading in patients with Parkinsonism (as estimated with NPG in Litvak et al. 2011, 2012). In this

429 paper we use an example recording in which NPG reveals a clear directed component from SMA →

430 STN. This recording was taken from a cohort of patients with PD who have undergone surgery for

431 deep brain stimulation (DBS). The experimental data contains recordings made using whole head

432 MEG and simultaneous LFP recordings from DBS electrodes implanted into the STN. The recordings

433    were made for approximately 3 minutes with the patient quietly at rest with their eyes open.

434    Experiments investigated the differences in MEG and LFP activity and connectivity when patients

435    were withdrawn from their usual dose of L-DOPA (OFF) versus the L-DOPA treated state (ON).

436    Patients were not undergoing stimulation with DBS at the time of the recording. The two-time series

437    analysed were 183s in duration with MEG from a right SMA virtual sensor recorded simultaneously

438    with an LFP from the right STN in a PD patient in the OFF state at rest. All experiments were

439    conducted in a study approved by the joint ethics committee of the National Hospital of Neurology

440    and Neurosurgery and the University College London Institute of Neurology. The patient gave their

441    written informed consent. For full details of the surgery, implantation, recording, and experimental

442    paradigm please see Litvak et al. 2011.

### 2.6.2  Preprocessing

444    The MEG and LFP signals were first down-sampled to 200 Hz. They were then preprocessed using a

445    high-pass filter (passband at 4 Hz, finite impulse response, two-pass, filter order optimized for data

446    length). Recordings were truncated 1s at either end to remove border artefacts arising due to

447    movement and equipment initialization. Finally, data were visually inspected to determine the

448    presence of large abnormalities and high amplitude transients. In the case of the example data used

449    here, none were found.

450    We performed estimation of the empirical SNR of the signals as detailed in section 2.4.2. The

451    empirical data was first standardized to unit variance and then spectral peaks in the 14-31 Hz were

452    compared with that of a white noise surrogate also with unit variance. The ratio between the peaks is

453    reported as the estimated empirical SNR, equivalent to the difference of the spectral peak (in beta

454    band) with that of the noise floor.

455    Changes to the SNR, asymmetric SNR, and linear mixing of the empirically derived signals were

456    introduced using the same process as listed in section 2.4.2. This treatment ignores the fact that the

457    data by necessity of empirical recording have already undergone observation with a transform similar

458    in form to that in equation (13) but with unknown parameters regarding the lead-field (mixing matrix)

459    and observation noise. Instead we take the empirical recordings as a ground-truth and investigate

460    subsequent changes following artificially induced confounds.

## 2.7  Statistics

### 2.7.1  Permutation Confidence Intervals

463    In order to form confidence intervals for the connectivity metrics we make no assumptions as to the

464    form of their distributions but instead form permutation distributions of the metrics estimated from

465    surrogate data and computed using a non-parametric rank order significance threshold (Theiler et al.

466    1992). We adopt a phase randomization approach to generate surrogates (Breakspear and Terry 2002;

Lancaster et al. 2018) which acts to preserve the magnitudes of the spectral estimates whilst scrambling the phase and hence disrupting any interaction between signals. For details and a discussion of the algorithm please see appendix I as well as Lancaster et al. (2018). For each test we generated 1000 realizations of the surrogate process. We obtain the P = 0.001 confidence limit by taking the 99.9[th] percentile of the resulting distribution. Limits are plot in figures as a dashed line with arrows on the side of the axis to indicate their values.

### 2.7.2 Least-Squares Regression

In the case of some confounds the response profiles were found to be sigmoidal functions with a maximum response, midpoint $x_0$; and steepness $\kappa$. We used a least-squares regression to fit the logistic function. All reported fits exceeded $R^2 > 0.95$ and we report the estimated parameters of the curves as summary statistics of the connectivity metrics' modulation by a confound.

## 3 Results

## 3.1 Organization of the Results

In the following section the effects of common drive, degradation of SNR, asymmetric SNR, instantaneous signal mixing, data availability, and simultaneous confounders upon estimation of dFC using NPD and NPG are investigated. In figures 1-4 examples of the impact of these individual confounding factors upon the power and connectivity spectra are presented. In order to summarise the effects of the confounds across a much larger range of scales, in figure 5 the effects of SNR, unequal SNR, and signal mixing are visualized as a plot of the relevant statistic of the connectivity (i.e. strength or asymmetry) against a scale of values of the confounding factor. In each of the following sections (3.2-3.5) we inspect first the example spectra displayed in figures 1-4, and then go on to establish the total effect over the full range of the confound using the data illustrated in figure 5. Figures 6 and 7 use a benchmarking approach to quantify the accuracy of recovery given differing data lengths and mixed confounds. In the final section and figure 9 we look at application of the metrics to empirically recorded data.

## 3.2 Effects of Lagged Dependencies and Common Drive

We first demonstrate the efficacy of the metrics at recovering simple hierarchical architectures and establish how common input can act to confound them. To this end we present results from a simple 3-state, 3rd order MVAR model with no signal mixing and zero observation noise. The MVAR model is imbued with periodic dynamics that are identical at each node and are driven by noise with fixed covariance structure. Non-zero (off-diagonal) matrix coefficients are all fixed at 0.5 and the full MVAR parameters can be seen in table 1 of appendix II. We design the MVAR model (figure 1A) such that all edges originate at node X and correlations are lagged such that an input arriving at node

500   Z lags that at node Y ($\delta_1 < \delta_2$). This introduces a deliberate confound as dFC methods estimating

501   causality in a way dependent upon temporal lag will assign spurious causality from Y to Z, due to the

502   difference in arrival times of input from X. An example time series of the process is shown in figure

503   1B and the resulting analyses of the functional connectivity are shown in figure 1C.

504   This model generates rhythmic activity at ~55 Hz as indicated by the peaked autospectrum for each

505   node. Functional connectivity as measured using standard coherence shows significant connectivity (>

506   0.5) between all nodes, albeit reduced for the connection between Y and Z. We next estimate directed

507   connectivity using NPD. NPD shows that all connections are in the forward direction for X → Y and

508   X → Z. As the full coherence is equal to the sum of the directional components, the overlap of the

509   forward NPD (spectra in the top-right panel of the figure) with the coherence shows that they are

510   equivalent in this case. The shorter lag in transmission from node X → Y compared to X → Z, results

511   in a spurious estimate of coupling from Y → Z when estimated with NPD. However, when we

512   condition the NPD upon the signal that both node X and Z receive common input from (NPD

513   conditioned on node X; NPD(X)), we see that the Y→ Z correlation is abolished.

514   When pairwise Granger (NPG) was applied to the simulated data, the connectivity from X to Z and Y

515   was very similar in form to the unconditioned NPD (data not shown). However, as the multivariate

516   estimator of Granger (mvNPG) considers the full covariance across all nodes, its application acted to

517   remove the spurious Y→ Z correlation that arose due to the common drive. This limitation of pairwise

518   NPD is readily overcome using the multivariate extension that allows for the conditioning of the

519   common input. In this way the results between mvNPG and NPD conditioned upon the common input

520   (NPD(X)) are comparable. Both NPD(X) and mvNPG give estimates of Y → Z that are below the P =

521   0.001 confidence interval indicating the absence of any significant directed connectivity between X

522   and Y.

## 3.3  Effects of Low Signal-to-Noise Ratios

524   Recordings of field activity in the brain are made in the presence of both endogenous neural

525   background activity as well as observer noise originating from recording equipment and other sources

526   outside the brain. In figure 2 we simulate the effects of signal-to-noise ratio (SNR) upon estimates of

527   functional connectivity. The variance of the MVAR process was standardized and so was equal in all

528   simulations. We used additive Gaussian noise in the observation model to simulate an SNR of 1:0 (+

529   ∞ dB), 4:3 (+ 5.3 dB), and 1:3 (- 1.0 dB). All functional connectivity metrics were resistant up to

530   moderate amount of additive noise ($SNR_{dB} = + 5.3$ dB), but all estimates were heavily attenuated for

531   the greatest noise tested in figure 2 i.e. SNR = -1.0 dB. When looking across a wider range of SNRs

532   (figure 5A), both NPD and NPG approached 0 when the data became almost entirely noise i.e. SNR

533   approached 0:1 (- ∞ dB). Responses were sigmoidal for all three metrics measured with half

534   maximum suppression around 50% signal loss. Non-linear least-squares fitting yielded parameter

535    estimates of the logistic rise for each FC estimator (midpoint $x_0$ and steepness $\kappa$): coherence $x_0^{Coh} =$

536    1.12 dB, $\kappa^{coh} = 0.12$; NPD $x_0^{NPD} = 1.47$ dB, $\kappa^{NPD} = 0.11$; and NPG $x_0^{NPG} = + 7.1$ dB, $\kappa^{NPG} = 0.07$.

537    From these estimates and the curves shown in figure 5A, it is clear that coherence and NPD

538    effectively share the same response profile to SNR. NPG is more sensitive to noise with estimates

539    becoming degraded at higher SNRs ($x_0^{NPG} > x_0^{NPD}$). Overall the two metrics have a difference in the

540    midpoints of the calibration curves of ~8 dB, with NPG being more sensitive to noise by almost an

541    order of magnitude greater than NPD. However, the differences between the NPG estimator and NPD

542    result in different SNR thresholds required to detect statistically significant connectivity (i.e. greater

543    than the P = 0.001 confidence threshold) and so the measures reach significance at different SNR

544    levels: for NPG at -7 dB (SNR = 1:5), and for NPD at -11.5 dB (SNR = 1:14).

## 3.4   Effects of Differences in Signal-to-Noise Ratios between Signals

546    Asymmetries in the SNR of different signals are known to distort the estimation of dFC when using

547    methods based upon Granger causality (Bastos and Schoffelen 2016; Nolte et al. 2008). We next

548    tested whether this was true for NPD. We simplified the model to contain just 2 nodes that were

549    reciprocally connected with the same lag. Again, the output of the MVAR model was standardized to

550    have unit variance. We then modified the SNR of the first node (X) via the same process as for the

551    previous set of simulations but fixing the variance of the noise of the second (Y) node to yield an SNR

552    of +13 dB. Signals were constructed with a difference of SNRs between X and Y ($\Delta SNR_{XY}$) equal to

553    -17 dB, -7 dB, and 0 dB and calculated with respect to the SNR of Y which was held constant. The

554    results of the simulations are shown in figures 3 and 5B. In figure 3 we plot the difference in the

555    estimates of the directed connection (i.e. X → Y minus Y → X; $\Delta FC_{XY}$) to explore any deviation

556    away from the symmetry in functional connectivity expected from the MVAR model ($\Delta FC_{XY} \approx 0$).

557    Our simulations confirm that NPG is biased by differences in SNR between signals, showing that

558    even at moderate asymmetries ($\Delta SNR_{XY}$ = -7 dB) the weaker signal is estimated to be driven by the

559    stronger i.e. Y→ X. NPD suffers far less from this confound and maintains estimation of the

560    difference in coupling as close to zero for all conditions tested. Analysis with NPD shows far less

561    deviation from the ground truth of symmetrical coupling when the SNRs are unequal. When looking

562    across a range of SNR asymmetries the response of each measure is apparent (figure 5B). NPG

563    spuriously identifies directed coupling, with the bias for Y leading when $\Delta SNR_{XY}$ is in the range -10

564    dB to -50 dB and peaking around -35 dB (zone II of figure 5B). In contrast, the bias for X leading is

565    when X has a stronger SNR and $\Delta SNR_{XY}$ is in range of +10db to +50 dB, and peaking around

566    $\Delta SNR_{XY} = +35$ dB (zone IV). At very large (positive) or very small (negative) $\Delta SNR_{XY}$ the bias in

567    coupling is diminished and there is a return to symmetrical estimate of connectivity as both NPD and

568    NPG approach 0 for both directions (zones I and V). However, whilst NPD exhibits a much weaker

569    bias than NPG it does still demonstrate an above significant difference in connectivity. However,

570    deviations in estimation of symmetrical coupling arising due to unequal SNR are roughly an order of

571    magnitude smaller than NPG with a maximum $\Delta NPD_{XY}$ of -0.045 versus $\Delta NPG_{XY}$ of -0.42. In terms

572    of deviation from the difference in measures when $\Delta SNR_{XY}$ = 0 dB, NPD shows a maximum of 1.5

573    times inflation in asymmetry. For NPG this bias is a maximum of 20 times larger indicating its

574    increased susceptibility to unbalanced SNRs.

## 3.5  Effects of Instantaneous Signal Mixing

576    Neurophysiologically recorded signals such as MEG, EEG, and LFPs are subject to instantaneous

577    mixing of the underlying dipole currents as a result of field spread effects. We next simulate these

578    effects by multiplication of the simulated MVAR process with a linear mixing matrix and investigate

579    the influence of mixing coefficients upon estimates of dFC. We use an identical model to that in

580    section 3.2 (3 state, 3rd order MVAR) but with the addition of the observer model to model signal

581    mixing at a range of values of λ to yield simulations with 0%, 20%, and 60% shared variance. There

582    is no observation noise added. The results of the analysis are shown in figure 4.

583    The confounding effect of instantaneous mixing was established by first estimating the degree to

584    which it may influence the symmetrical zero-lag component of the NPD. As expected, it was found

585    that the zero-lag NPD is increased by mixing (data not shown), particularly at frequencies outside of

586    the periodic component of the signal. This occurs as in the case of the unmixed signals, correlation

587    between processes is dictated by off diagonal MVAR coefficients at lags greater than zero. When

588    mixing is introduced, common noise from outside the main frequency band of interaction more

589    readily overcomes the intrinsic noise at each node (which is weaker in power than activity at the

590    interaction frequency) and so results in the largest zero-lag correlations outside of the main periodic

591    component of the signals.

592    When using NPD to estimate dFC we found that it accurately reconstructs the designed connectivity

593    up to a moderate degree of signal mixing (45% shared variance), albeit with a reduction of the

594    estimated magnitude of connectivity (e.g. 0.6 to 0.4 for X → Y). At the highest degree of mixing

595    (90% shared variance) the spurious connectivity between nodes Y and Z (introduced by the lagged

596    common drive from node X) becomes increasingly symmetrical with an increase in the connectivity

597    in the reverse direction (i.e. Y → X) despite the absence of these connections in the model arising

598    either by design or by lagged common input. Overall, with increased signal mixing, the estimate of

599    NPD is weakened equally across all connections. Analysis with NPG however shows that mixing has

600    the effect of introducing spurious connectivity between Y and Z, exhibiting a small but significant

601    reversal connectivity at Z → Y at even moderate mixing (45% shared variance). At the greatest

602    degree of mixing, NPG determines statistically significant connections (above P = 0.001 permutation

603    confidence interval) for Y → X and Z → X, neither of which are in the underlying model. Unlike

604    NPD, which shows a uniform reduction in magnitude with increased mixing, the magnitude of NPG

West et al. (2018): A Novel Non-Parametric Directionality Measure                    **v5.3**

Journal Pre-proof

605   estimates depends upon the initial SNR of the nodes. In this instance the X → Z connection is
606   weakened whilst the X → Y is strengthened. This effect is due to the process explored in section 3.4,
607   by which unequal SNR biases the NPG estimator.

608   When testing across a wider range of degrees of signal mixing (figure 5C) the difference in the
609   response of NPD and NPG is apparent. When using NPG to estimate dFC the magnitude of the
610   estimate of X→ Y increases to a maximum at around 50% shared variance and then quickly collapses
611   at very high mixing as instantaneous correlations begin to predominate. This result is related to the
612   findings of the section 3.4 in which it was shown that signal leakage acts to modify the effective SNR
613   of the signals such that leakage from one signal can act to bias causality estimates towards another
614   signal at even moderate amounts of instantaneous mixing. This effect is apparent when looking at the
615   trace of the standard (symmetrical) coherence (in blue) which drops to a minimum at ~30% shared
616   variance but then increases as zero-lag correlations take over. As the NPD explicitly ignores the zero-
617   lag component, it displays simpler behaviour, and reduces in amplitude with increased mixing. This
618   occurs because zero-lag coherence predominates, and the lagged components become increasingly
619   small.

## 3.6  Effects of Data Availability upon Benchmarks of the Metrics'
##       Accuracy

622   Application of functional connectivity metrics to real world data are often limited by the amount of
623   data that is available to estimate them. In the next series of analyses, we quantify the dependency of
624   accurate estimation upon the sufficiency of the given data. We use the benchmarking approach laid
625   out in the methods and examine the role of data availability in two ways: 1) data which is continuous
626   but of fixed total length (500s) data which is variable in length but with a fixed trial length. The
627   results of this are shown in figure 6. In figure 6 A and B we compare NPD with mvNPG in the
628   accurate recovery of known patterns of connectivity using a benchmark score of accuracy (see method
629   section 2.5) when using a fixed amount of data. We observe a common trend that the overall accuracy
630   of recovery increases with trial length, reaching a maximum at the highest trial length tested at $2^{10}$
631   samples (equivalent to 39 trials each ~5s in duration assuming a 200 Hz sampling rate).  The recovery
632   of denser models required longer trial lengths and overall were estimated less accurately. This effect
633   occurs due to the introduction of common drive effects inducing false-positive detection of
634   connections. Sparser networks including just one single connection reached maximum accuracy with
635   trial lengths as short as $2^5$ samples (equivalent to 1250 trials each ~0.16s in duration). With a fixed
636   data length, it was found that NPD required shorter trials than mvNPG to reach similar degrees of
637   accuracy (figure 6A versus 6B). Accuracy of recovery falls off with longer duration trials as the
638   reduced number of repetitions hinders accurate estimation.

639 In figures 6 C and D, the total data availability (i.e. 100 trials of variable duration) upon estimator
640 accuracy was investigated. Again, both metrics displayed improved accuracy with increasing trials
641 lengths. However, with longer trial lengths, mvNPG was able to accurately recover connectivity of
642 models with denser connectivity than for NPD: in the case of networks with three random
643 connections, and with a long trial length of $2^{10}$, mvNPG reached ~85% benchmark score versus 65%
644 for NPD. Sparser models with just one or two connections showed an optimal trial length around $2^5$
645 (0.16s at 200 Hz) for mvNPG versus $2^6$ (0.32s at 200 Hz) for NPD.

## 3.7 Effects of Combined Confounds: Instantaneous Mixing and Asymmetric Signal-to-Noise Ratios

648 Empirically recorded signals are subject to several simultaneous confounding effects. In figure 7 we
649 present results from a benchmarking analysis in which we confound simulated signals by introducing
650 both asymmetric signal to noise, as well as instantaneous mixing of sources to a range of combined
651 degrees. In figure 7A and 7B we compare the performance of mvNPG and NPD in the estimation of
652 connectivity in MVAR models with one random connection. We vary instantaneous mixing from 0 to
653 100% shared variance; and asymmetric SNR at -45 dB to 0 dB. These simulations show that when
654 estimating connectivity using NPD in sparse networks with just a single connection there is a highly
655 accurate recovery (>95% benchmark scores) unaffected by asymmetric SNR, and only with high
656 shared variance (> 50%) is there any significant drop in accuracy. A combination of strong
657 asymmetry (-30 dB) and high mixing can however reduce benchmark scores to 30%. In comparison,
658 mvNPG demonstrates poor accuracy across a much wider area of the conditions tested - with the
659 benchmark reduced from 100% to 20% in the presence of negative asymmetric SNR greater than -20
660 dB (i.e. source node is weakest) and at all degrees of mixing above 20%. Benchmark scores are
661 weakened further by the coincidence of strong instantaneous mixing of the signals.

662 In figures 7 C and D we vary instantaneous mixing from 0 to 100% shared variance; and asymmetric
663 SNR at -45 dB to 0 dB.  These tests show that mvNPG is more readily corrupted by both confounds
664 with scores ranging from 80% to 50% along the asymmetric SNR axis, and from 80% to -10% along
665 the axis in which instantaneous mixing is varied. Furthermore, the estimation of denser connectivity
666 with NPD is hindered by asymmetric SNR but is less susceptible to combined signal mixing. Whereas
667 the negative benchmark scores for mvNPG indicate common detection of false positives, scores for
668 NPD do not drop below 40% for any of the combined confounds tested.

## 3.8 Confounds for Conditioned Directed Connectivity Arising from Incomplete Measurement of Signals.

671 We next investigate the properties of the multivariate extension to NPD which we term *conditioned*
672 NPD.  Conditioned dFC provides a more powerful method with which to explore network functional

673 connectivity; however, in empirical cases, conditioning with a tertiary signal Z may not produce

674 complete attenuation of the spuriously inferred directed connection between X and Y arising from the

675 common input Z. This may arise as a result of: i) incomplete capture of the activity occurring at Z;

676 and/or ii) difference in the routing of signals; and/or iii) because there are other sources of the

677 spuriously inferred connection than Z alone. In cases where structural connectivity is well understood,

678 and the conditioned signal Z is not expected to interconnect the path between nodes X and Y, any

679 attenuation when conditioning can be assumed to arise in information propagated forward in the

680 network (feedforward). On the other hand, if anatomical connectivity is unclear the effect of

681 conditioning upon directed connectivity may also be explained by conventional serial routing (i.e. X

682 $\to Z \to$ Y) but with incompleteness of observed signals at Z resulting in only partial attenuation of the

683 X $\to$ Y estimate. In the next set of tests, we ask whether there are any differences in how the

684 measures of dFC behave in the face of incomplete signal observation.

685 For this set of simulations, we use a three state, $3^{rd}$ order MVAR model, with all nodes generating

686 identical autonomous dynamics and identical cross-node coefficients at equal model lags. We test

687 three model connectivities to compare three types of signal propagation: a) serial (i.e. X $\to Z \to$ Y); b)

688 feedforward (i.e. X $\to$ Y $\to$ Z); or c) recurrent (i.e. X $\to$ Y $\to$ Z $\to$ X). We simulate incomplete

689 observation of Z by modifying the SNR as was done in section 3.2. The model architectures and

690 results of simulations are shown in figure 8. We demonstrate that in the simplest case of a serial path,

691 the NPD conditioned on signal Z (NPD(Z)) behaves as expected: the estimate of connectivity X $\to$ Y

692 is attenuated as all information between them is routed via Z. With decreasing SNR of the observation

693 of Z we show that conditioning has less and less effect and converges to the estimate yielded by the

694 unconditioned NPD. Pairwise NPD remains constant at all SNRs tested as it does not account for any

695 of the activity at Z. In these simulations, multivariate NPG (mvNPG) was also applied as a way to

696 estimate directed connectivity that accounts for all signals in the model. We find that mvNPG shows a

697 small decrease (~0.025) in the estimate of X $\to$ Y with increased SNR of Z. This weak attenuation

698 demonstrates that mvNPG can detect serial routing, yet it is not as suited for discriminating direct

699 connectivity (i.e. X $\to$ Y) from when there is relay via a secondary node (X $\to Z \to$ Y).

700 We next looked at a feedforward network, where X propagates directly to Y, but is then relayed on to

701 Z. Because some of the information passed X $\to$ Y is contained in Z, we expect conditioning to

702 attenuate the directed connection. Again, we find that NPD(Z) behaves as expected, although the

703 attenuation is weaker than in (A) when Z mediated the routing entirely. In this way the difference in

704 values between the NPD and NPD(Z) yields a measure of how much information of X is fed forward

705 from Y $\to$ Z. Thus, decreasing SNR of the observation of Z decreases the attenuating effect of the

706 conditioned NPD. mvNPG remains at a constant magnitude for all SNRs tested. This demonstrates

707 that the multivariate estimator of Granger causality is not sensitive to feedforward configurations

West et al. (2018): A Novel Non-Parametric Directionality Measure     **v5.3**

Journal Pre-proof

708    whereby the estimation of connectivity between X and Y is not influenced by activity at the terminal
709    (receiving) node.

710    For the third test, we investigated the combination of recurrent loops in the network and incomplete
711    signal observation- two features likely to occur in real recordings from neural systems. We find that
712    with complete signal observation (i.e. SNR $\rightarrow \infty$) the metrics behave similarly to the feedforward
713    model. A notable difference is the increased NPD of X $\rightarrow$ Y compared to the feedforward case, as
714    correlations are reinforced by signals resonating across the loop. NPD(Z) behaves in a similar way as
715    before, showing attenuation of the conditioned estimate at low noise levels, but converging back to
716    the unconditioned NPD as the reference signal is obscured by noise and estimation of its confounding
717    influence is lost. The mvNPG estimate of the connection X $\rightarrow$ Y decreases by 0.1 as the observation
718    noise of Z is reduced. This finding indicates that in the case of recurrent connectivity, mvNPG is
719    sensitive to the quality of the signal recorded at the routing node. In the case of recurrent
720    configurations, this finding shows that mvNPG can readily discriminate between direct X $\rightarrow$ Y
721    connectivity and cyclical routing via a secondary signal recorded at Z.

## 3.9 Example of Estimation of Directed Functional Connectivity in Confounded Empirical Data: Cortico-Subthalamic Connectivity

724    Using the example dataset described in section 2.6 we examine how changes in the overall SNR,
725    differences in SNR between signals, and instantaneous signal mixing may act to confound the
726    estimation of dFC in empirical data recorded from simultaneous MEG and LFP in patients with
727    Parkinson's disease. We first analyse the original empirical data and then subsequently introduce
728    synthetic confounding effects as described in the methods section that outlined observation modelling.
729    The results of this analysis are presented in figure 9.

730    We demonstrate in the original data that there is a clear asymmetry in coupling with both NPD and
731    NPG indicating a clear dFC from SMA $\rightarrow$ STN. The zero-lag component (top row figure 9) of the
732    NPD is negligible in the original data. In contrast, the instantaneous component of NPG shows above
733    significance level connectivity at 20-30 Hz. The empirical SNR of the data was estimated using the
734    method described in section 2.6.2. We use activity in the beta band (14-30 Hz) to define the signal and
735    then compare with the noise floor. SNR estimates of the MEG virtual electrode and LFP were + 1.9
736    dB (SNR$_{SMA}$ $\approx$ 3:2) and + 4.0 dB (SNR$_{STN}$ $\approx$ 5:2) respectively. This yields an empirical $\Delta SNR$ of -2.1
737    dB with the LFP measured at the STN having the largest SNR.

738    In the first set of experiments we reduced the SNR of both signals equally (figure 9 A-C). We added
739    noise to the original signals to yield a range of SNRs: + $\infty$ dB, + 4.1 dB, and -1.9 dB. These analyses
740    show that both NPG and NPD estimates of connectivity respond to a uniform reduction in SNR in a

741    simple and predictable way by reducing their overall magnitude approaching zero as the signals

742    become mostly noise.

743    Subsequently, the effect of changing the SNR of only one of the signals upon dFC estimates was also

744    investigated (figure 9 D-F). Signals were constructed to have a range of $\Delta SNR$: - 3 dB; +16 dB; and +

745    26 dB. We reduced the SNR of the strongest signal only (STN; $SNR_{dB}^{STN}$), in an attempt to bias the

746    directionality estimates in the reverse direction (i.e. increase the strength of STN → SMA). However,

747    it was found for both NPD and NPG that this had a similar effect to reducing the SNR symmetrically

748    (i.e. when SMA → STN is weakened). This result suggests that for this dataset, it may not be possible

749    to induce a strong bias in the inferred dFC by making one signal weaker than the other (i.e.

750    $SNR_{dB}^{SMA} >> SNR_{dB}^{STN}$) as there is no anatomical STN→SMA feedback (a situation in contrast with

751    simulations investigating asymmetric SNR in section 3.4.).

752    In the final column of figure 9 (panels G-I) the effect of signal mixing was measured. We simulated

753    several degrees of signal mixing: λ = 0 (0% shared variance); λ = 0.075 (7.5% shared variance); and λ

754    = 0.15 (15% shared variance). Again, it was found that the instantaneous component of the NPD

755    behaves as expected, increasing in magnitude with increased signal mixing. This is most apparent in

756    the frequencies outside the main oscillatory bands of activity. When using the instantaneous part of

757    NPG, we found that there was generally an increase, yet the frequencies around the main component

758    (of the peak in the lagged connectivity) were negative and uninterpretable. Furthermore, we show that

759    even moderate increases in the signal mixing (7.5%) corrupt the dFC estimation when using NPG.

760    This is especially apparent at high mixing levels (15%), where a wide band reverse component

761    (STN→SMA) arises, as well as large second peak in the SMA→STN at around 4-12 Hz. NPD

762    estimates are much more stable in comparison and only show a reduction in the original peak with

763    increased mixing, but no spurious peaks emerge outside of this range at any of mixing degrees tested.

# 4    Discussion

765    The results presented in this paper further support the NPD methodology as an accurate and robust

766    method for the estimation of dFC in continuous neural data. We first provided a face validation of

767    NPD for estimation of the directed interactions between MVAR processes. Secondly, we assessed the

768    performance of the NPD measure in the presence of several confounding factors that are likely to

769    arise in experimental recordings of neurophysiological networks, namely: volume conduction,

770    common drive, low SNR, unequal SNRs between signals, and recurrent connectivity. Thirdly, we

771    provided a direct comparison of NPD with a well-established estimate of dFC based on Granger

772    causality – NPG. Finally, our results show that the additional information gained from using a

773    conditioned, multivariate extension of the NPD method allows for some of the confounding

774    influences of common drive, or non-trivial signal routing, to be mitigated. The degree to which this is

775 achieved is dependent upon the extent to which the signal captures the neural activity at the recording
776 site.

## 4.1 A Summary of Effects of Signal Confounds

### 4.1.1 Effects of Common Drive

779 Common input to two parallel neural populations has long been known to be a confounding factor
780 when estimating functional connectivity (Aertsen et al. 1989; Farmer et al. 1993; Horwitz 2003). The
781 limitations of finite sampling over the brain means that no FC measure is immune to this problem as
782 there always remains the potential for an unmeasured common input to the recorded populations from
783 which an FC estimate is made. Our simulations demonstrate this effect where both pairwise NPD and
784 NPG estimates indicate spurious causality in the case of lagged common input. However, when using
785 multivariate extensions of the two methods, in which the common drive signal is factored out, it is
786 possible to avoid spurious estimation of connectivity between nodes sharing a common drive. This is
787 shown to be true when using the multivariate NPG which accounts for the total covariance across the
788 network. On the other hand, NPD in its simplest form is measured in a pairwise manner and cannot
789 account for the action of a tertiary signal on the naïve estimate. However, we demonstrate that this
790 issue can be remedied using the multivariate extension of NPD in which the influence of a common
791 drive may be regressed out in order to eliminate spurious connectivity between the driven nodes.
792 Whilst this is a solution when the common drive is observed, there still remains the potential
793 confound of an unobserved common signal, to which NPD and NPG are equally susceptible. These
794 issues can be addressed by model based estimators of effective connectivity such as dynamic causal
795 modelling which allow for the inference of unobserved states in a causal network (Friston et al. 2013).

### 4.1.2 Effects of A/symmetric Signal-to-Noise Ratios

797 Functional connectivity estimates are subject to the limits of inference implied by the SNR of the
798 available recordings. We demonstrate (figure 5A) that coherence, NPD, and NPG are degraded by
799 poor SNR with similar logistic decays. However, NPG exhibits a greater susceptibility to degradation
800 by noise than NPD. NPG magnitude are reduced at SNRs an order of magnitude higher than those that
801 would elicit an equal reduction in NPD. Despite this, both measures show a remarkable resistance to
802 even high levels of noise, with the range of SNRs at which both NPG and NPD provide statistically
803 significant estimates of connectivity (i.e. having a magnitude exceeding the P = 0.001 confidence
804 interval) reaching as low as SNR = 1:30 (equivalent to -15 dB). This would suggest that both are
805 robust to the occurrence of false-negative errors as a result of poor SNR in neural recordings. These
806 findings can also explain the common empirical finding of significant functional connectivity in the
807 absence of obvious peaks in the power spectra.

West et al. (2018): A Novel Non-Parametric Directionality Measure     v5.3

Journal Pre-proof

808    A number of authors have noted that estimation of Granger causality is biased by the existence of

809    unequal SNRs (Bastos and Schoffelen 2016; Haufe et al. 2013; Nolte et al. 2008). Our simulations

810    reiterate this fact and demonstrate that NPG is biased to estimate the driving node as the strongest

811    signal (section 3.4; figure 5B). This is an important problem as all neurophysiological signals

812    comprise some unknown mixture of the signal of interest and background noise on a source by source

813    basis. As a result, it can rarely be assumed that the SNRs of two signals are balanced. We find that

814    when investigating the simultaneous effects of unequal SNR and instantaneous mixing, that NPG is

815    most easily corrupted by the asymmetry in the signals, whereas NPD is most sensitive to mixing.

816    This is particularly important when looking at directed connectivity between signals recorded from

817    two different modalities (e.g. MEG and LFP) where the estimate will be biased in favour of the higher

818    gain recording (to lead). For instance, in our data we show a difference in empirical SNRs of 4.5 dB

819    between the LFP and virtual channel signals. This has led some authors to suggest the usage of time-

820    reversed data as surrogate comparison for dFC methods (Haufe et al. 2013) because if a true causal

821    effect is present then time reversal should flip the sign of the directionality. Future validations should

822    explore whether this approach can reduce the susceptibility of the NPD method to so called "weak"

823    data asymmetries. However, the simulations here demonstrate that estimates made using NPD are far

824    less subject to this confound than NPG. NPD is still affected by decreased SNR (both asymmetric and

825    symmetric) but shows no bias, as directional estimates decrease uniformly as the SNR goes down.

826    This finding leads us to suggest that in future studies of dFC in multimodal data or in other cases

827    where the signals are likely to be of differing SNR, the NPD method provides a more robust and

828    readily interpretable result over Granger based approaches.

### 4.1.3   Effects of Simulated Volume Conduction through Signal Mixing

830    The extent to which signals recorded from the brain are subject to the influence of volume conduction

831    is generally more severe with decreasing distance between the recording electrodes. Experiments have

832    demonstrated that LFPs measured from electrodes separated by a distance of 5 cm will typically show

833    $R^2$ values indicating approximately 50% shared variance (Nunez et al. 1997) and so analyses of

834    directed functional connectivity are likely to be significantly affected by instantaneous mixing at

835    distances much closer than this (e.g. recordings made from neighbouring contacts of the same

836    intracranial electrodes). Instead, some authors have shown that functional connectivity analyses are

837    better suited to source localized signals due to the reduced extent of signal leakage (Schoffelen and

838    Gross 2009). This is likely to hold true for the application of NPD analysis to whole brain recordings.

839    It is difficult to find a limit for when zero-lag effects will corrupt a method such as NPG as this

840    ultimately depends on the nature of the lagged connectivity present in the data. In our simulations, we

841    show that the bias on NPG induced by mixing is dependent upon the original SNR of the signals as a

842    result of confounding by the mechanism of SNR asymmetry discussed in the previous section.

West et al. (2018): A Novel Non-Parametric Directionality Measure | v5.3

Journal Pre-proof

843  In addition to the benefit of being less susceptible to corruption by volume conduction, NPD provides
844  explicit frequency resolved estimation of the zero-lag component of coherence, making it possible to
845  estimate the extent to which coupling is influenced by instantaneous effects. This characteristic
846  affords NPD an advantage over corrected methods of FC such as imaginary coherence or the phase
847  locking index (Nolte et al. 2004; Vinck et al. 2011) which are set up to ignore zero-phase coherence.
848  In this respect it is important to note that zero-phase coherence can reflect synchronous physiological
849  coupling  (Roelfsema et al. 1997). We also note that volume conduction is manifest not only through
850  the mixing of known sources of interest, but also hidden sources (Bastos and Schoffelen 2016). This
851  introduces a confound like that of limited signal observation (see below) in which the influence of a
852  node can only be estimated if it is directly observable.

### 4.1.4  Effects of Data Length on Estimation Accuracy

854  Estimation of connectivity in empirical data is limited by the availability of recorded data due either
855  to experimental design or practical limitations of storage and acquisition. In figure 6 we presented a
856  set of tests to determine the sensitivity of the two methods to data length. Overall, we find that NPG is
857  the most robust of the two and can make accurate recovery at trial lengths two orders (to the power of
858  2) shorter than NPD. As expected, this exact effect is dependent upon the complexity of the model to
859  be evaluated. In the case where more dense networks are to be estimated, the required amount of data
860  is larger than for simpler models with one or two connections. These limitations are likely due to the
861  variance of the spectral estimators from which the two metrics are decomposed, with coherence
862  known to be sensitive to having a larger number of samples to restrict estimates.

863  It is well known that insufficient sampling will hinder parametric estimators of Granger causality
864  (Seth et al. 2015). Simulations here suggest that with a good number of trial repetitions (> 35) at a
865  sampling rate of 200 Hz, trial lengths from 0.5 to 1 second are required for accurate estimation with
866  NPD. For NPG, this requirement is reduced to a minimum of 0.2 seconds, although these guidelines
867  are likely to depend upon the SNR, as well as frequency band of the interaction of interest in the
868  analysed data.

### 4.1.5  Effects of Limited Signal Observation

870  The argument that conditioned metrics of dFC such as conditioned NPD provide an increased ability
871  to infer the causal structure of real-world neural networks hinges upon the assumption that a recorded
872  signal truly captures the complete dynamics of the underlying population through which the signal is
873  routed. In section 3.8 we provide an analysis of how the incomplete observation of signals acts to
874  confound the estimates of dFC under several hypotheses of signal propagation: A) serial; B)
875  feedforward; and C) recurrent connectivity (figure 8). In the case of the simplest architecture - serial
876  propagation, the metrics behave as expected – the more poorly the signal used to perform the
877  conditioning captures the underlying dynamics, the less the conditioning can inform accurate

West et al. (2018): A Novel Non-Parametric Directionality Measure     **v5.3**

Journal Pre-proof

878    estimation of directed connectivity. In the case of complete signal capture, the conditioning procedure

879    (NPD(Z)) completely attenuates the directed connection ($X \rightarrow Y$), as there is no possibility that any of

880    the information contained in Y concerning node X is exclusive of Z. Therefore, if the signal recorded

881    at Z completely captures the dynamics of Y then there is the potential to attenuate the $X \rightarrow Y$

882    connection entirely using a conditioning on Z. In the case of feedforward propagation, conditioning

883    will also act to attenuate the estimate, but unlike serial processing (where the reference node Z

884    provides an intermediate node in the chain of propagation between X and Y) the attenuation can never

885    be complete as the variance introduced at Z is not shared with X or Y. In case C we show that the re-

886    entrant connection acts to increase the overall coherence due to cyclical passage of information in the

887    circuit. Furthermore, conditioning acts to bring the NPD estimate closer to that of the feedforward

888    model (where the re-entrant connection is missing). In the case of recurrent connectivity, the

889    multivariate NPG also acts to discount the reconnection via Z. When Z is completely captured (SNR

890    is high) then the NPG gives an estimated connectivity equivalent again to the feedforward model.

891    These observations make it clear that if conditioning removes the inferred connectivity in its entirety

892    then the conditioned node must be in a relay like position (i.e. $X \rightarrow Z \rightarrow Y$). For instance, this was

893    found to be the case in West et al. (2018) where conditioning of NPD between the striatum and

894    subthalamic nucleus upon the external segment of the globus pallidus removed connectivity almost

895    entirely, leading to the conclusion that information propagated serially in the network, a finding in-

896    line with known anatomical details of the indirect pathway of the basal-ganglia. However, the

897    findings described in the present paper regarding the combination of circuit organization and SNR of

898    conditioned signals introduce ambiguity when interpreting the results of conditioned or multivariate

899    estimates of directed connectivity in empirical data. For instance, incomplete attenuation of

900    conditioning may arise either from poor SNR of the reference signal in a serial network or may

901    indicate that the conditioned signal is placed in either a feedforward or recurrent configuration. In this

902    case it is necessary to combine evidence from multiple conditioning steps (e.g. also conditioning $X \rightarrow$

903    $Z$ on $Y$) in order to determine the exact signal routing. Previous work has argued that additive noise

904    only impairs estimation rather than distorts temporal structure of the signals (Baccalá and Sameshima

905    2006), here we show that this disruption is dependent upon the exact routing of the signals.

906    Specifically, in networks containing a high degree of reciprocity, partialized estimated of coherence

907    (both directed and undirected) are likely to be confounded. This finding could be used in principle to

908    further specify the role of a conditioned node by determining its effect upon directed connectivity in

909    response to additive noise.

## 910   4.2   Extensions and Final Conclusions

911    We have presented a validation of NPD, a novel tool for the assessment of dFC, in continuous neural

912    recordings such as that measured in methods commonly used for human neuroimaging. We argue that

913 in the face of common practical issues arising from the physical limitations of many experimental
914 recording methods, as well as from the complex biology of the systems that they aim to explore, NPD
915 and its conditioned extension provide a useful method that builds upon the founding principles of the
916 more established Granger causality. The NPD measure (conditioned and unconditioned) has been
917 recently demonstrated to provide insights into the patterns of propagating neural activity in animal
918 electrophysiology in the basal-ganglia (West et al. 2018) and hippocampus (Halliday et al. 2016); as
919 well as in human motor networks (Halliday 2015; Spedden et al. 2019). and is likely to have wide
920 application across other domains of clinical and experimental neuroscience. The finding that NPD is
921 robust to the confounding effects of SNR asymmetry means that it may be readily applied to multi-
922 modal neural recordings without some of the concerns that may arise with Granger-based methods.

923 The validation provided here is not extensive: there is a wide range of other existing dFC metrics to
924 which we have not made comparison, and so it is possible that other metrics may perform better than
925 NPG (for an extensive comparison of many metrics, not including NPD, see Wang et al. 2014).
926 Granger causality-based methods have become a staple of the dFC toolbox and form the statistical
927 foundation for several methods developed since including the directed transfer function (Kaminski
928 and Blinowska 1991) and partial directed coherence (Baccalá and Sameshima 2001). An adaptation of
929 the directed transfer function aimed at improving estimation of directed connectivity (i.e. $X \rightarrow Y$)
930 introduced by Korzeniewska et al. 2003 may perform better at recovering known patterns of
931 connectivity in the face of common drive than the metrics presented here. Furthermore, the role of
932 time reversal procedures (Haufe et al. 2013) in alleviating some of these shortcomings in the metrics
933 should be the subject of future study. This is likely to be important when investigating more complex
934 networks or high dimensional data such as that measured with magneto- or electroencephalographic
935 recordings. However, NPD shows broadly equivalent results to the Granger based measure but
936 exhibits more robust performance in the recovery of complex network topologies in highly
937 confounded data. The full extent to which this is true either in networks of a greater size or density
938 will need to be tested.

939 We conclude that the NPD measure of directed functional connectivity is inexpensive to compute,
940 makes limited assumptions of the properties of the data, is flexible to the form of the original spectral
941 estimate and is conceptually simple to formulate. It eschews the computationally expensive estimation
942 of model parameters required for parametric estimates of Granger causality or directed transfer
943 function and doesn't require iterative binning procedures such as that use in information-based
944 metrics like transfer entropy. Overall, NPD provides a simple and compact statistical description of
945 directed dependencies between signals and is readily interpretable, providing the basis for testable
946 hypotheses of causation in real neural systems.

West et al. (2018): A Novel Non-Parametric Directionality Measure **v5.3**

Journal Pre-proof

947  ## 5    Acknowledgements

951  ## 6    Funding

957  ## 7    Competing Interests

958  The authors have no competing interests to declare.

959  ## 8    Bibliography

960  **Aertsen AM**, **Gerstein GL**, **Habib MK**, **Palm G**. Dynamics of neuronal firing correlation:

961  modulation of "effective connectivity." *J Neurophysiol* 61: 900–917, 1989.

962  **Baccalá LA**, **Sameshima K**. Partial directed coherence: a new concept in neural structure

963  determination. *Biol Cybern* 84: 463–474, 2001.

964  **Baccalá LA**, **Sameshima K**. Comments on 'Is Partial Coherence a Viable Technique for Identifying

965  Generators of Neural Oscillations?' *Biol Cybern* 95: 135–141, 2006.

966  **Bastos AM**, **Schoffelen J-M**. A Tutorial Review of Functional Connectivity Analysis Methods and

967  Their Interpretational Pitfalls. *Front Syst Neurosci* 9: 175, 2016.

968  **Breakspear M**, **Terry JR**. Detection and description of non-linear interdependence in normal

969  multichannel human EEG data. *Clin Neurophysiol* 113: 735–753, 2002.

970  **Bressler SL**, **Seth AK**. Wiener–Granger Causality: A well established methodology. *Neuroimage* 58:

971  323–329, 2011.

972  **Brillinger DR**. Time series: data analysis and theory [Online]. Holt, Rinehart, and

973  Winston.https://books.google.co.uk/books?id=9hzvAAAAMAAJ.

974  **Brillinger DR**. Some Statistical Methods for Random Process Data from Seismology and

West et al. (2018): A Novel Non-Parametric Directionality Measure **v5.3**

Journal Pre-proof

975      Neurophysiology. *Ann Stat* 16: 1–54, 1988.

976      **Brovelli A**, **Ding M**, **Ledberg A**, **Chen Y**, **Nakamura R**, **Bressler SL**. Beta oscillations in a large-
977      scale sensorimotor cortical network: Directional influences revealed by Granger causality. *Proc Natl*
978      *Acad Sci U S A* 101: 9849–9854, 2004.

979      **Cui J**, **Xu L**, **Bressler SL**, **Ding M**, **Liang H**. BSMART: A Matlab/C toolbox for analysis of
980      multichannel neural time series. *Neural Networks* 21: 1094–1104, 2008.

981      **Dhamala M**, **Rangarajan G**, **Ding M**. Analyzing information flow in brain networks with
982      nonparametric Granger causality [Online]. *Neuroimage* 41: 354–362,
983      2008ahttps://www.sciencedirect.com/science/article/pii/S1053811908001328 [19 Sep. 2016].

984      **Dhamala M**, **Rangarajan G**, **Ding M**. Estimating Granger Causality from Fourier and Wavelet
985      Transforms of Time Series Data. *Phys Rev Lett* 100: 018701, 2008b.

986      **Ding M**, **Chen Y**, **Bressler SL**. Granger Causality: Basic Theory and Application to Neuroscience.
987      In: *Handbook of Time Series Analysis*. Wiley-VCH Verlag GmbH & Co. KGaA, p. 437–460.

988      **Farmer SF**, **Bremner FD**, **Halliday DM**, **Rosenberg JR**, **Stephens JA**. The frequency content of
989      common synaptic inputs to motoneurones studied during voluntary isometric contraction in man. *J*
990      *Physiol* 470: 127–55, 1993.

991      **Friston K**, **Moran R**, **Seth AK**. Analysing connectivity with Granger causality and dynamic causal
992      modelling. *Curr Opin Neurobiol* 23: 172–178, 2013.

993      **Friston KJ**. Functional and Effective Connectivity: A Review. *Brain Connect* 1: 13–36, 2011.

994      **Geweke J**. Measurement of Linear Dependence and Feedback Between Multiple Time Series. *J Am*
995      *Stat Assoc* 77: 304, 1982.

996      **Goldenholz DM**, **Ahlfors SP**, **Hämäläinen MS**, **Sharon D**, **Ishitobi M**, **Vaina LM**, **Stufflebeam**
997      **SM**. Mapping the signal-to-noise-ratios of cortical sources in magnetoencephalography and
998      electroencephalography. *Hum Brain Mapp* 30: 1077–86, 2009.

999      **Granger CWJ**. Investigating Causal Relations by Econometric Models and Cross-spectral Methods.
1000    *Econometrica* 37: 424, 1969.

1001    **Halliday D**, **Rosenberg JR**, **Amjad A**, **Breeze P**, **Conway BA**, **Farmer SF**. A framework for the
1002    analysis of mixed time series/point process data—Theory and application to the study of physiological
1003    tremor, single motor unit discharges and electromyograms. *Prog Biophys Mol Biol* 64: 237–278,
1004    1995.

1005    **Halliday DM**. Nonparametric directionality measures for time series and point process data. *J Integr*

West et al. (2018): A Novel Non-Parametric Directionality Measure **v5.3**

Journal Pre-proof

1006    *Neurosci* 14: 253–277, 2015.

1007    **Halliday DM**, **Senik MH**, **Stevenson CW**, **Mason R**. Non-parametric directionality analysis –
1008    Extension for removal of a single common predictor and application to time series. *J Neurosci*
1009    *Methods* 268: 87–97, 2016.

1010    **Haufe S**, **Nikulin V V.**, **Müller K-R**, **Nolte G**. A critical assessment of connectivity measures for
1011    EEG data: A simulation study. *Neuroimage* 64: 120–133, 2013.

1012    **Haufe S**, **Nikulin V V**, **Nolte G**. Alleviating the Influence of Weak Data Asymmetries on Granger-
1013    Causal Analyses. In: *Latent Variable Analysis and Signal Separation*, edited by Theis F, Cichocki A,
1014    Yeredor A, Zibulevsky M. Berlin, Heidelberg, Heidelberg: Springer Berlin Heidelberg, 2012, p. 25–
1015    33.

1016    **Horwitz B**. The elusive concept of brain connectivity. *Neuroimage* 19: 466–470, 2003.

1017    **Kamiński M**, **Ding M**, **Truccolo WA**, **Bressler SL**. Evaluating causal relations in neural systems:
1018    Granger causality, directed transfer function and statistical assessment of significance. *Biol Cybern*
1019    85: 145–157, 2001.

1020    **Kaminski MJ**, **Blinowska KJ**. A new method of the description of the information flow in the brain
1021    structures. *Biol Cybern* 65: 203–210, 1991.

1022    **Korzeniewska A**, **Mańczak M**, **Kamiński M**, **Blinowska KJ**, **Kasicki S**. Determination of
1023    information flow direction among brain structures by a modified directed transfer function (dDTF)
1024    method. *J Neurosci Methods* 125: 195–207, 2003.

1025    **Lancaster G**, **Iatsenko D**, **Pidde A**, **Ticcinelli V**, **Stefanovska A**. Surrogate data for hypothesis
1026    testing of physical systems. *Phys Rep* 748: 1–60, 2018.

1027    **Litvak V**, **Eusebio A**, **Jha A**, **Oostenveld R**, **Barnes G**, **Foltynie T**, **Limousin P**, **Zrinzo L**, **Hariz**
1028    **MI**, **Friston K**, **Brown P**. Movement-related changes in local and long-range synchronization in
1029    Parkinson's disease revealed by simultaneous magnetoencephalography and intracranial recordings. *J*
1030    *Neurosci* 32: 10541–53, 2012.

1031    **Litvak V**, **Jha A**, **Eusebio A**, **Oostenveld R**, **Foltynie T**, **Limousin P**, **Zrinzo L**, **Hariz MI**, **Friston**
1032    **K**, **Brown P**. Resting oscillatory cortico-subthalamic connectivity in patients with Parkinson's
1033    disease. *Brain* 134: 359–374, 2011.

1034    **Lütkepohl H**. Stable Vector Autoregressive Processes. In: *New Introduction to Multiple Time Series*
1035    *Analysis*. Springer Berlin Heidelberg, p. 13–68.

1036    **Nalatore H**, **Ding M**, **Rangarajan G**. Mitigating the effects of measurement noise on Granger
1037    causality. *Phys Rev E* 75: 031123, 2007.

1038    **Newbold P**. Feedback Induced by Measurement Errors. *Int Econ Rev (Philadelphia)* 19: 787, 1978.

1039    **Nolte G**, **Bai O**, **Wheaton L**, **Mari Z**, **Vorbach S**, **Hallett M**. Identifying true brain interaction from

1040    EEG data using the imaginary part of coherency. *Clin Neurophysiol* 115: 2292–307, 2004.

1041    **Nolte G**, **Ziehe A**, **Nikulin V V.**, **Schlögl A**, **Krämer N**, **Brismar T**, **Müller K-R**. Robustly

1042    Estimating the Flow Direction of Information in Complex Physical Systems. *Phys Rev Lett* 100:

1043    234101, 2008.

1044    **Nunez PL**, **Srinivasan R**, **Westdorp AF**, **Wijesinghe RS**, **Tucker DM**, **Silberstein RB**, **Cadusch**

1045    **PJ**. EEG coherency: I: statistics, reference electrode, volume conduction, Laplacians, cortical

1046    imaging, and interpretation at multiple scales. *Electroencephalogr Clin Neurophysiol* 103: 499–515,

1047    1997.

1048    **Oostenveld R**, **Fries P**, **Maris E**, **Schoffelen J-M**, **Oostenveld R**, **Fries P**, **Maris E**, **Schoffelen J-**

1049    **M**. FieldTrip: Open Source Software for Advanced Analysis of MEG, EEG, and Invasive

1050    Electrophysiological Data. *Comput Intell Neurosci* 2011: 1–9, 2011a.

1051    **Parkkonen L**. Instrumentation and data preprocessing. *MEG An Introd to methods* 24–64, 2010.

1052    **Pereda E**, **Quiroga RQ**, **Bhattacharya J**. Nonlinear multivariate analysis of neurophysiological

1053    signals. *Prog Neurobiol* 77: 1–37, 2005.

1054    **Pierce DA**. Signal Extraction Error in Nonstationary Time Series. *Ann Stat* 7: 1303–1320, 1979.

1055    **Richter CG**, **Coppola R**, **Bressler SL**. Top-down beta oscillatory signaling conveys behavioral

1056    context in early visual cortex. *Sci Rep* 8: 6991, 2018.

1057    **Roelfsema PR**, **Engel AK**, **König P**, **Singer W**. Visuomotor integration is associated with zero time-

1058    lag synchronization among cortical areas. *Nature* 385: 157–161, 1997.

1059    **Sayed AH**, **Kailath T**. A survey of spectral factorization methods. *Numer Linear Algebr with Appl* 8:

1060    467–496, 2001.

1061    **Schoffelen J-M**, **Gross J**. Source connectivity analysis with MEG and EEG. *Hum Brain Mapp* 30:

1062    1857–1865, 2009.

1063    **Seth AK**, **Barrett AB**, **Barnett L**. Granger Causality Analysis in Neuroscience and Neuroimaging. *J*

1064    *Neurosci* 35: 3293–3297, 2015.

1065    **Spedden ME**, **Jensen P**, **Terkildsen CU**, **Jensen NJ**, **Halliday DM**, **Lundbye-Jensen J**, **Nielsen**

1066    **JB**, **Geertsen SS**. The development of functional and directed corticomuscular connectivity during

1067    tonic ankle muscle contraction across childhood and adolescence. *Neuroimage* 191: 350–360, 2019.

1068    **Sporns O**. Networks of the Brain [Online]. MIT

West et al. (2018): A Novel Non-Parametric Directionality Measure **v5.3**

Journal Pre-proof

1069 Press.https://books.google.co.uk/books?id=v1DBKE7-UrYC.

1070 **Srinivasan R**, **Winter WR**, **Ding J**, **Nunez PL**. EEG and MEG coherence: Measures of functional
1071 connectivity at distinct spatial scales of neocortical dynamics. *J Neurosci Methods* 166: 41–52, 2007.

1072 **Swanson LW**. Brain Architecture: Understanding the Basic Plan [Online]. OUP
1073 USA.https://books.google.co.uk/books?id=4rAlwYWVEroC.

1074 **Theiler J**, **Eubank S**, **Longtin A**, **Galdrikian B**, **Doyne Farmer J**. Testing for nonlinearity in time
1075 series: the method of surrogate data. *Phys D Nonlinear Phenom* 58: 77–94, 1992.

1076 **Truccolo WA**, **Ding M**, **Knuth KH**, **Nakamura R**, **Bressler SL**. Trial-to-trial variability of cortical
1077 evoked responses: implications for the analysis of functional connectivity. *Clin Neurophysiol* 113:
1078 206–226, 2002.

1079 **Vinck M**, **Oostenveld R**, **van Wingerden M**, **Battaglia F**, **Pennartz CMA**. An improved index of
1080 phase-synchronization for electrophysiological data in the presence of volume-conduction, noise and
1081 sample-size bias. *Neuroimage* 55: 1548–1565, 2011.

1082 **Wang HE**, **Bénar CG**, **Quilichini PP**, **Friston KJ**, **Jirsa VK**, **Bernard C**. A systematic framework
1083 for functional connectivity measures. *Front Neurosci* 8: 405, 2014.

1084 **Wen X**, **Rangarajan G**, **Ding M**. Multivariate Granger causality: an estimation framework based on
1085 factorization of the spectral density matrix. *Philos Trans R Soc A Math Phys Eng Sci* 371: 20110610–
1086 20110610, 2013.

1087 **West TO**, **Berthouze L**, **Halliday DM**, **Litvak V**, **Sharott A**, **Magill PJ**, **Farmer SF**. Propagation of
1088 Beta/Gamma Rhythms in the Cortico-Basal Ganglia Circuits of the Parkinsonian Rat. *J Neurophysiol*
1089 jn.00629.2017, 2018.

1090 **Wiener N**. Nonlinear Prediction and Dynamics [Online]. In: *Proceedings of the Third Berkeley*
1091 *Symposium on Mathematical Statistics and Probability, Volume 3: Contributions to Astronomy and*
1092 *Physics*. University of California Press, p. 247–
1093 252.https://projecteuclid.org/euclid.bsmsp/1200502197.

1094 **Zalesky A**, **Breakspear M**. Towards a statistical test for functional connectivity dynamics.
1095 *Neuroimage* 114: 466–470, 2015.

# 9 Figures

## 9.1 Figure 1(COLOR)
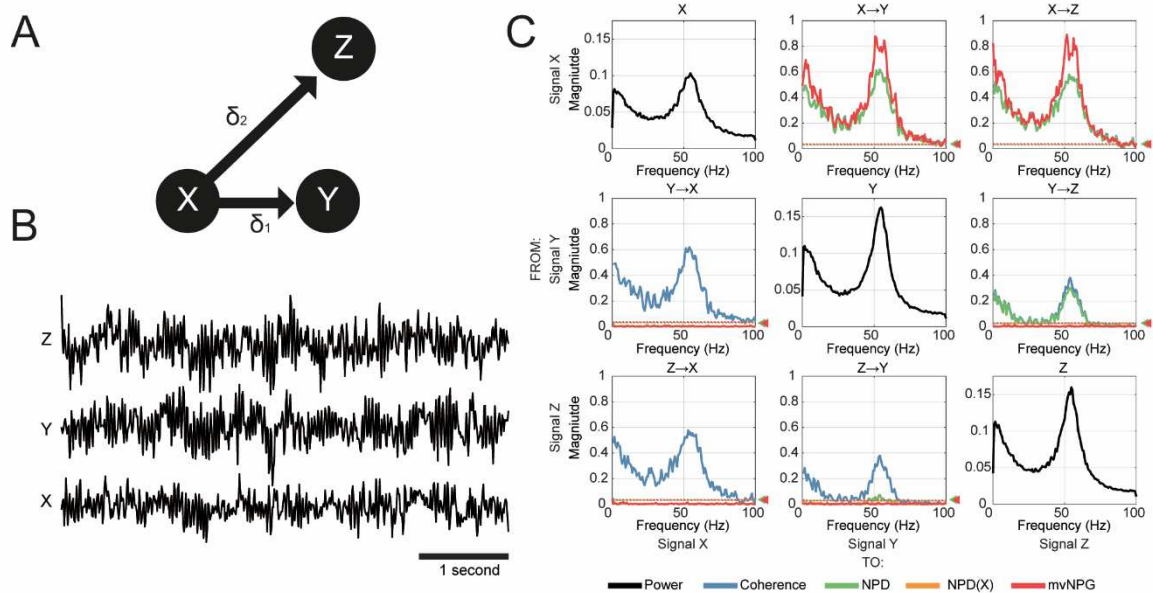


**Figure 1** – **Three -node simulation of MVAR model to compare functional connectivity measures**. **(A)** A simple three state, $3^{rd}$ order MVAR model was used to simulate coupling of autonomous periodic signals. Connectivity was simulated using non-zero coefficients at lag 2 for node X → Y, and lag 3 for X → Z. Correlations are lagged such that the time delays are unequal (i.e. $\delta_1 <$ $\delta_2$). **(B)** Example 5-second realization of the simulated MVAR processes. **(C)** Connectivity matrix of the coupled signals. Autospectra are shown on the diagonal (black). Undirected functional connectivity (coherence) is shown in blue. Estimates of directed connectivity are shown for multivariate non-parametric Granger causality (mvNPG; red); Non-parametric Directionality (NPD; green); and NPD conditioned on signal X (NPD(X); orange). NPD identifies spurious directional connectivity between Y and Z due to the lagged correlations of X → Y relative to X → Z. Spurious connectivity is removed partializing the NPD estimate upon the signal at the common source at node X (NPD(X)) which acts to remove all spurious connectivity. Permutation confidence intervals (P = 0.001) are shown for NPD and mvNPG by the green and red dashed lines and arrows respectively.

West et al. (2018): A Novel Non-Parametric Directionality Measure                    **v5.3**

Journal Pre-proof

## 9.2 Figure 2 (COLOR)
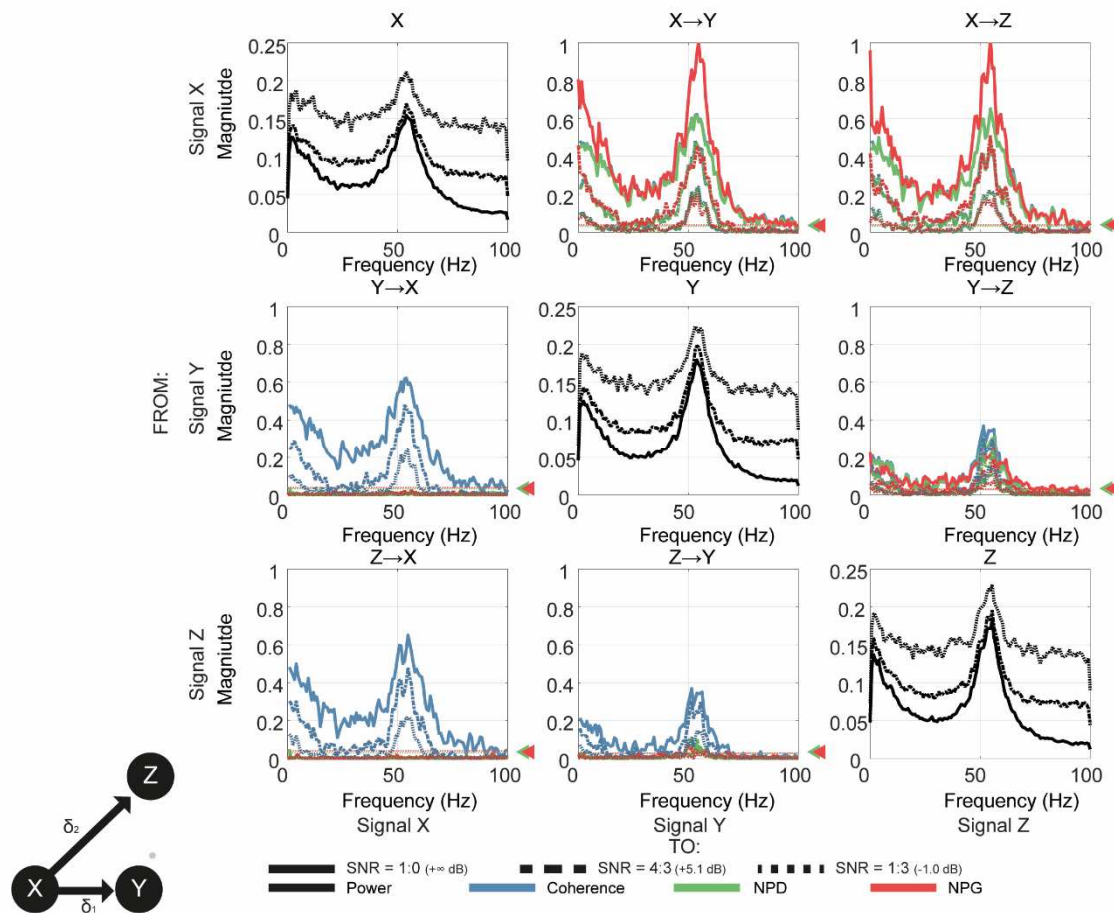


**Figure 2** – **Analysis of the effects of signal-to-noise ratio (SNR) upon estimators of directed functional connectivity.** The confounding effects of poor SNR were simulated by adding Gaussian noise to the MVAR processes and standardizing the overall variance equal to 1. The MVAR model is identical in form to that used in figure 1 and its structure is given by the ball and stick diagram in the inset. Simulated narrowband (45-55 Hz) SNRs at: 1:0 (+ ∞ dB; bold), 4:3 (+ 5.3 dB; ---), and 1:3 (-1.0 dB; ···). The effects upon coherence (blue), NPD (green), and non-parametric Granger causality (NPG) were investigated. All estimators were reduced by increased levels of noise. Permutation confidence intervals (P = 0.001) are shown for NPD and NPG by the green and red dashed lines and arrows respectively.

## 9.3 Figure 3 (COLOR)

1125



1126
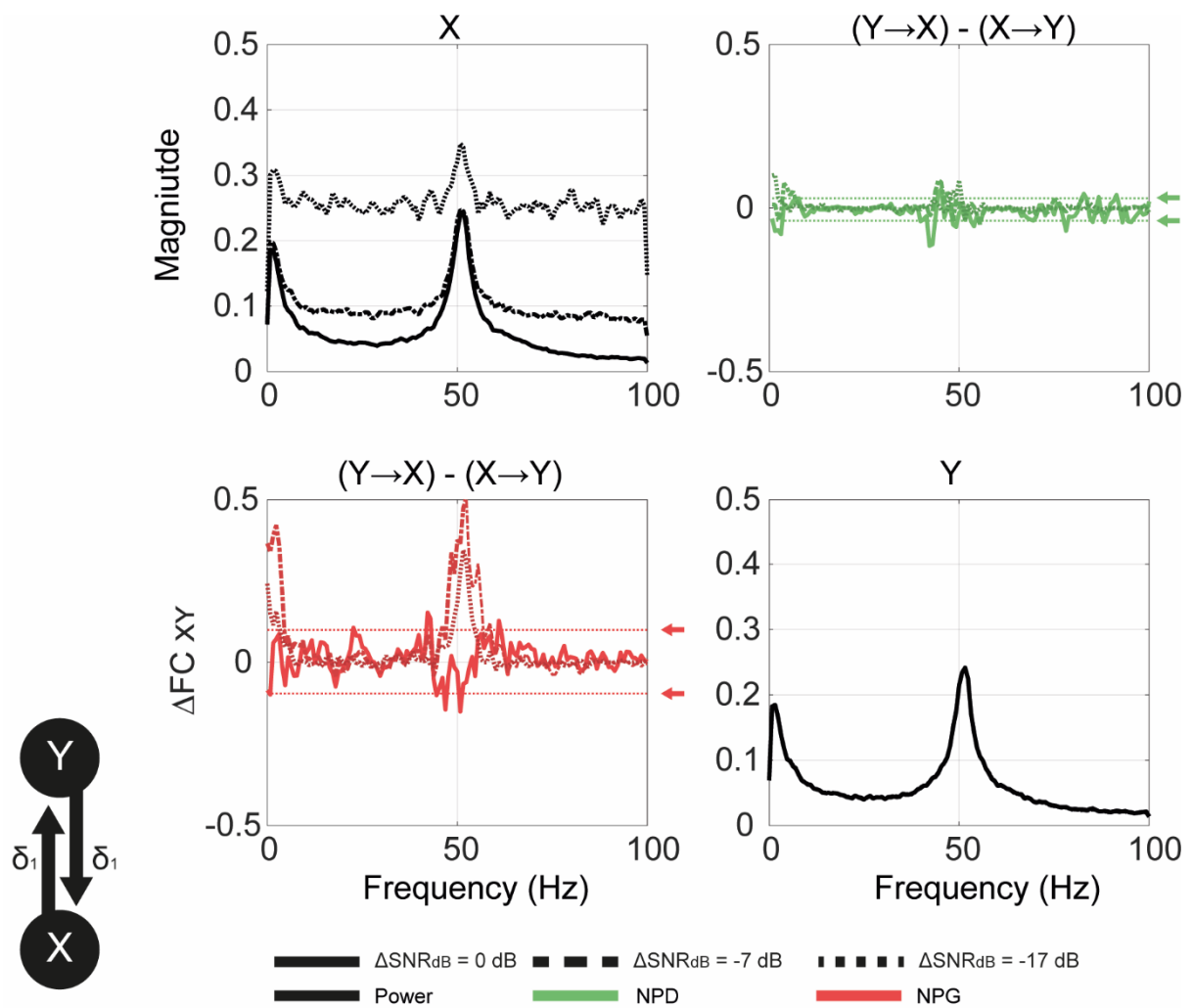
**Figure 3 – Analysis of the effects of unequal signal-to-noise ratios, measured as a difference of the SNRs between X and Y ($\Delta SNR_{XY}$) upon symmetrical directed functional connectivity (dFC).** The confounding effect of connected signals having different SNRs was simulated by the addition of Gaussian noise to signal X but fixing the noise of node Y to yield + 13 dB. A range of differences in SNR between X and Y ($\Delta SNR_{XY}$) were simulated at 0 dB (bold), - 7 dB (---), and - 17 dB (···). Connectivity was held fixed to be symmetrical. We assessed dFC by plotting the difference in magnitudes of the connectivity for each direction ($\Delta FC_{XY}$) with $\Delta FC_{XY} \approx 0$ as the ground truth. Results from both non-parametric directionality (NPD; green) and non-parametric Granger causality (NPG; red) are shown. In the face of medium amounts of SNR asymmetry, NPG spuriously identifies the strongest signal as the driving node. NPD suffers less from this issue and yields approximately symmetrical estimates for all conditions tested.

## 9.4 Figure 4 (COLOR)
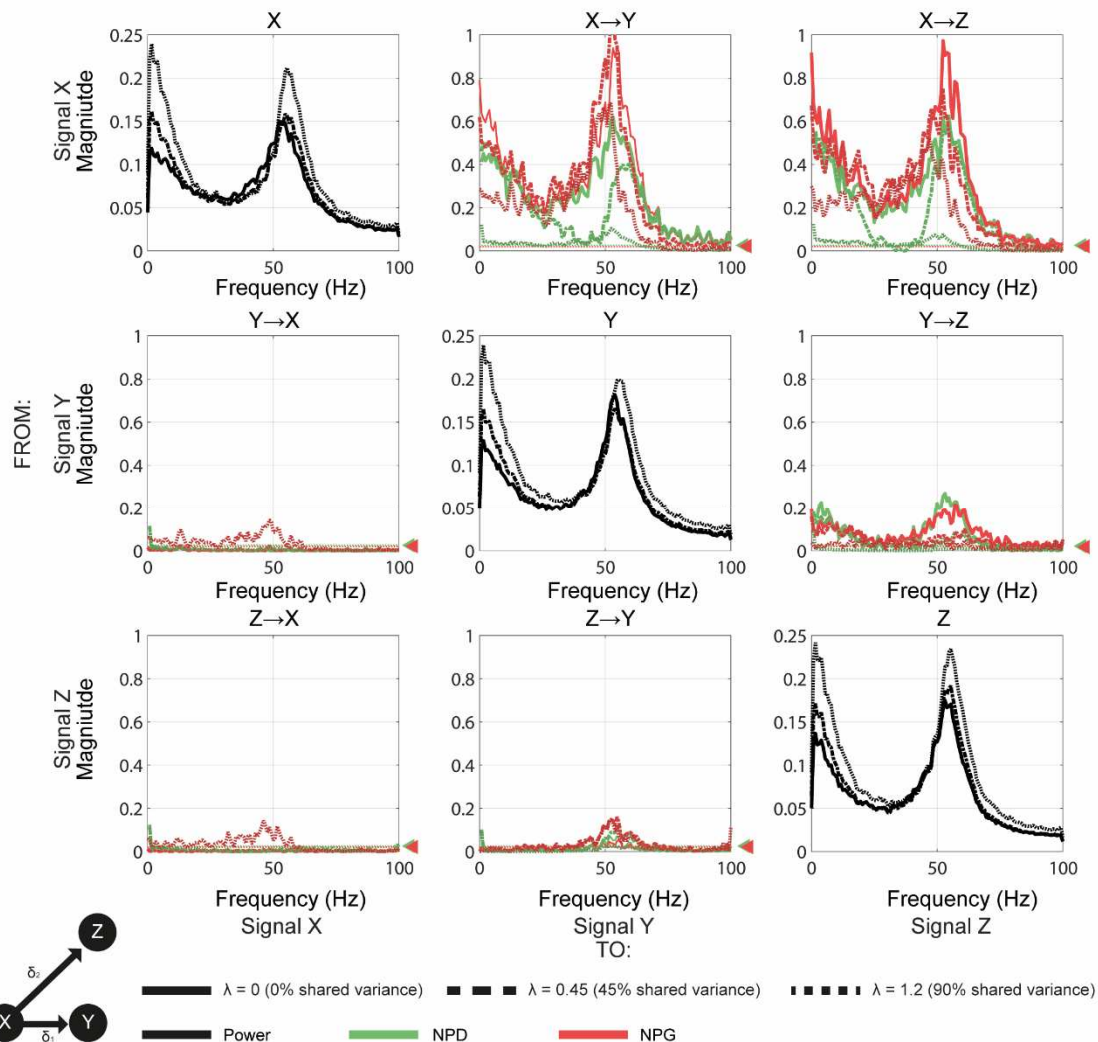


**Figure 4 – Analysis of the effects of instantaneous mixing upon estimates of directed functional connectivity (dFC).** The confounding effects of volume conduction were simulated by multiplication of signals with a mixing matrix with off-diagonal coefficients λ. The unmixed signals were first generated with a three state, $3^{rd}$ order MVAR model (identical to that used in figures 1 and 2). We simulate three mixing conditions: λ = 0 (zero mixing; bold line), λ = 0.45 (45% shared variance; ---), and λ = 1.2 (90% shared variance; ···). dFC is estimated using the lagged components of the NPD (green) or non-parametric Granger (NPG) (red). Permutation confidence intervals (P = 0.001) are shown for NPD and NPG by the green and red dashed lines and arrows respectively.

## 9.5 Figure 5 (COLOR)
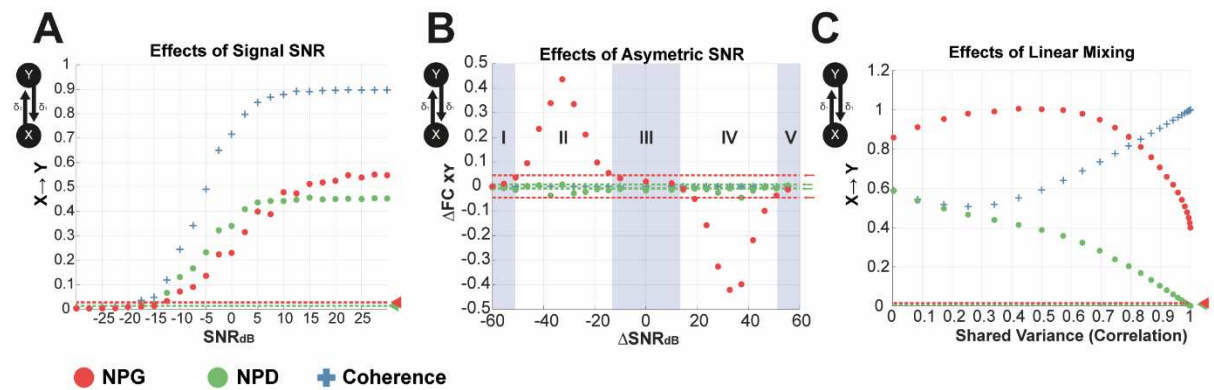


**Figure 5 – Investigating the effects of signal-to-noise ratios (SNR), SNR asymmetries, and instantaneous linear mixing upon functional connectivity measures: coherence (blue), non-parametric directionality (NPD; green), and non-parametric Granger causality (NPG; red).** All measures are reported as the peak value for each individual estimate. Permutation confidence intervals (P = 0.001) are shown for NPD and NPG by the green and red dashed lines and arrows respectively. **(A)** The effect of SNR was tested in the range from -30 dB to +30 dB. All estimators were found to have a sigmoidal response, with half-maximal suppression around SNR = 0 dB. **(B)** The effect of unequal SNR between nodes X and Y ($\Delta SNR_{XY}$) was varied by addition of observation noise to node X or Y separately to yield a range of narrowband $\Delta SNR_{XY}$ from -60 dB to + 60 dB whilst coupling strengths were held fixed. NPG incorrectly identifies asymmetrical coupling for a wide range of $\Delta SNR_{XY}$ (within zone II from -50 dB to -10 dB as well as zone IV from +10 dB to 50 dB). NPD estimates a weak bias towards one signal leading but with differences in directionality remaining close to zero across the range examined. **(C)** The effect of instantaneous signal mixing was examined across a range of mixing coefficients (λ) to yield a range of 0% to 100% shared variance. Coherence is shown to increase as zero-lag correlations predominate with increasing valued λ. The lagged NPD shrinks to zero as instantaneous component of coherence dominates. NPG increases to a maximum at around 65% signal mixing and then sharply falls to zero. Permutation confidence intervals (P = 0.001) are shown for NPD and NPG by the green and red dashed lines and arrows respectively.
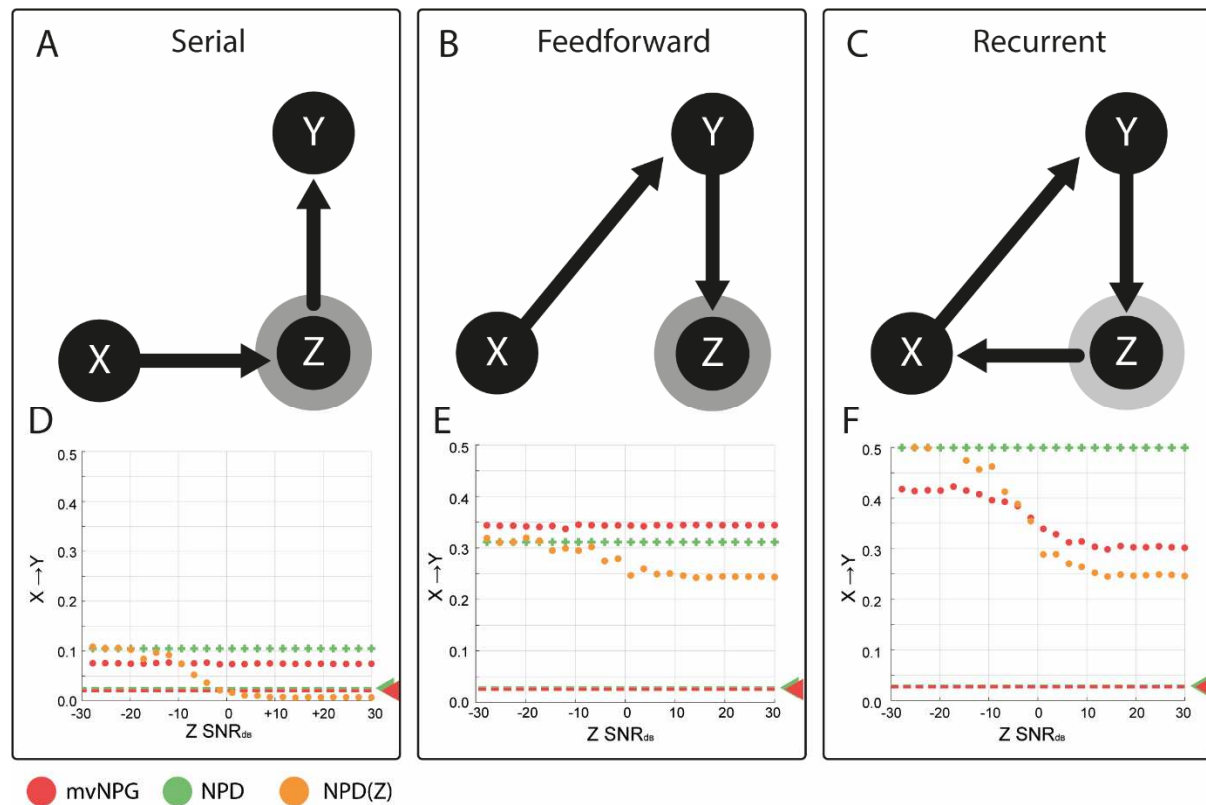
1169  ## 9.6  Figure 6 (COLOR)



1170
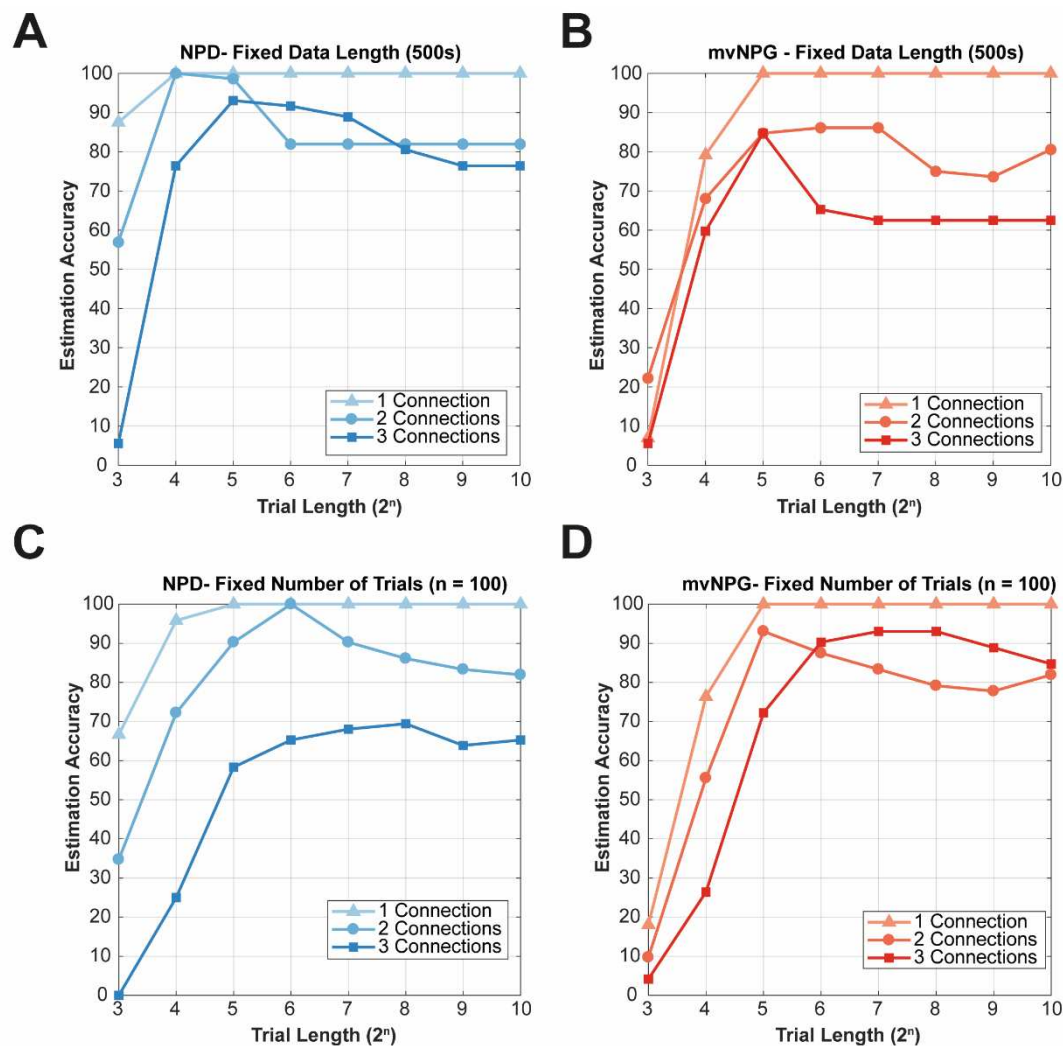
**Figure 6 – Investigating the role of data availability upon the accuracy of connectivity recovery when using non-parametric directionality (NPD; blue), and non-parametric Granger causality (NPG; red).** The two estimators were benchmarked against three sets of 24 MVAR models with random connectivity comprising either one, two, or three connections respectively. Different amounts of data were simulated for each model and the accuracy of the recovery was scored using the criteria set out in the methods. Simulated data is sampled at 200 Hz. **(A and B)** Benchmarks recorded from analyses of simulated data in which there was a fixed amount of data (500s) but allowing for variable trial lengths (in samples). **(C and D)** Benchmarks recorded from analyses of simulated data in which there were a fixed number of trials (n = 100) but variable total data length.

## 9.7 Figure 7 (COLOR)
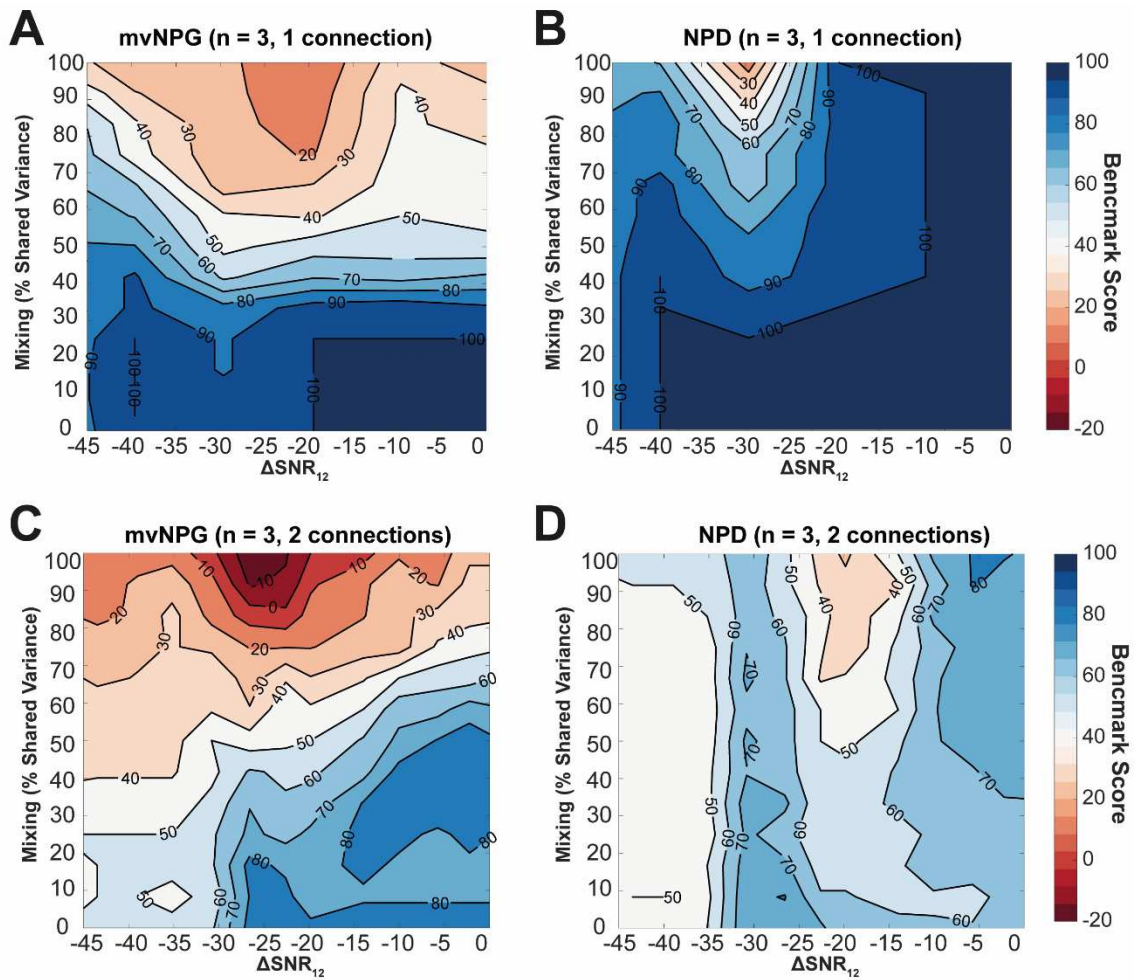


**Figure 7 – Investigating the role of combined data confounds (instantaneous mixing and asymmetric signal-to-noise ratio; $\Delta SNR_{XY}$) upon the accuracy of connectivity estimation when using non-parametric directionality, and non-parametric multivariate Granger causality.** The two measures were benchmarked against two sets of 24 realizations of a 3-node MVAR models comprising either one (top row), or two (bottom row) randomly placed connections. For each simulation 200s of data was simulated and divided into epochs of $2^8$ samples. Simulated data is sampled at 200 Hz. All data is represented as a contour plot when varying first instantaneous mixing from 0% to 100% shared variance; and then adjusting the approximate asymmetric narrowband (45-55 Hz) SNR from -45 dB to 0 dB. **(A)** Benchmarking of mvNPG with simulations containing one randomly placed connection on a three-node network. **(B)** Same as for (A) but using NPD. **(C)** Benchmarking of mvNPG with simulations containing two randomly placed connections on a three-node network. **(D)** Same as for (C) but using NPD as the estimator.

West et al. (2018): A Novel Non-Parametric Directionality Measure v5.3

Journal Pre-proof

## 9.8 Figure 8 (COLOR)



Figure 8 – **The effects of incomplete signal observation upon estimation of directed functional connectivity: non-parametric Granger causality (NPG); non-parametric directionality (NPD); and NPD conditioned on reference signal Z (NPD(Z)).** Simulations investigate the connectivity of $X \rightarrow Y$ and the influence of propagation involving a tertiary node Z. We simulate incomplete sampling of Z by modifying its signal-to-noise ratio (SNR) via the addition of Gaussian white noise and then standardizing the variance equal to 1. **(A and D) Serial propagation –** signals propagate from $X \rightarrow Z \rightarrow Y$. The results of changing the SNR of Z are shown in panel D. Simulations demonstrate that dFC estimation with NPD/NPG are constant. At complete signal observation (SNR 1:0; $+\infty$ dB), conditioning removes the estimate of dFC. With increasing SNR, the attenuation is diminished to the point where conditioning has no effect. **(B and E) Feedforward connectivity –** signals propagate to feedforward to the tertiary node: $X \rightarrow Y \rightarrow Z$. We find that conditioning has a weak effect (panel E), and the attenuation of NPD(Z) for estimation of $X \rightarrow Y$ is again reduced by decreasing SNR of Z. **(C and F) Recurrent connectivity –** a further connection is added to the model to complete a cyclic path in the network: $X \rightarrow Z \rightarrow Y \rightarrow X$. Decreasing the SNR of Z results in an increased estimation of NPG in $X \rightarrow Y$ (panel F). We again find that that increased completeness of observation of Z results in an increase in the efficacy of NPD(Z) in determining tertiary (non-direct) signal routing.

## 9.9 Figure 9 (COLOR)
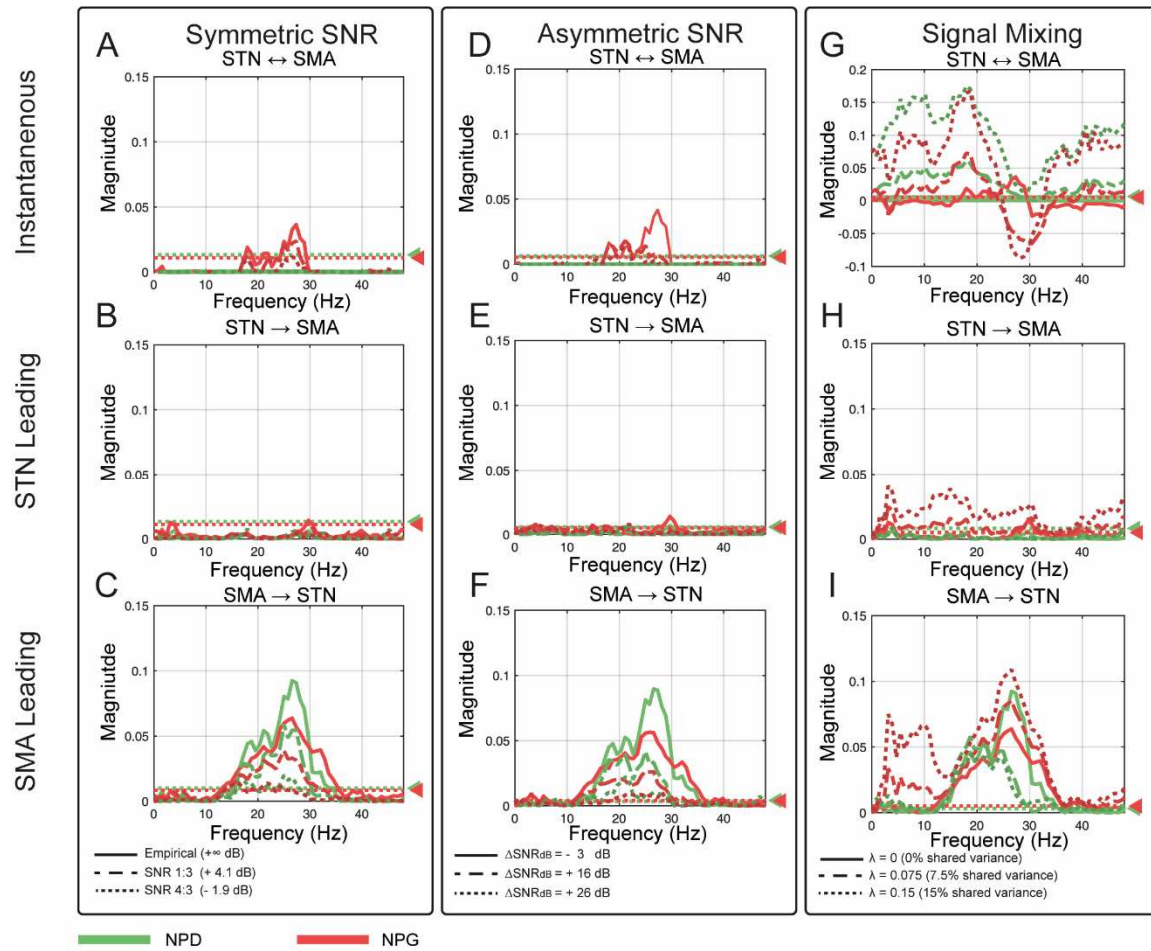


**Figure 9** – **Testing for the confounding effects of symmetric and asymmetric SNR, and instantaneous signal mixing upon estimation of directed functional connectivity in experimental data recorded in patients with Parkinson's disease.** Empirical data is comprised of local field potentials recorded from the STN and a virtual electrode localized to the SMA, computed from whole-head magnetoencephalography. Signals were analysed for dFC using the instantaneous components (first row); STN → SMA (second row); and SMA → STN (third row) parts of the NPD (green) and NPG (red). Empirical data is indicated by bold line; low by the dotted (⋯); and high degrees by the dashed (---). **(A-C)** The effect of modulating the overall SNR of the signals equally. We used a range of narrowband (14-31 Hz) SNRs: 1:1 (+ ∞ dB; bold); 4:3 (+ 4.1 dB; ---); and 1:3 (-1.9 dB; ⋯). **(D-F)** The effect of modulating the SNR of the strongest signal (STN) only. We used a range of $\Delta SNR$: -3 dB (bold); + 16 dB (---); and + 26 dB (⋯). **(G-I)** The effect of modulating the degree of instantaneous mixing between signals. We simulated a degree of signal mixing: $\lambda = 0$ (0% shared variance; bold); $\lambda = 0.075$ (7.5% shared variance; ---); and $\lambda = 0.15$ (15% shared variance; ⋯).

# 10 Appendices

## 10.1 List of External Toolboxes Used in Analysis, Statistics, and Plotting

1.  BSMART toolbox- Hualou Liang, Steven Bressler, Mingzhou Ding (Cui et al. 2008): http://www.brain-smart.org/
2.  Fieldtrip toolbox- Donders Insitute, Radboud University (Oostenveld et al. 2011a): www.fieldtriptoolbox.org/
3.  Linspecer - David Kun: https://github.com/davidkun/linspecer
4.  Neurospec 2.11 toolbox- David Halliday, University of York: http://www.neurospec.org/
5.  SPM 12 toolbox- UCL, Wellcome Centre for Human Neuroscience: https://www.fil.ion.ucl.ac.uk/spm/

## 10.2 Table of MVAR Coefficients

| Simulating Common Drive, Signal-to-noise, instantaneous mixing (figure 1, 2, 4, 5C) | |
| --- | --- |
| *Transfer Matrix* | *Noise Covariance Matrix* |
| $A_1 = \begin{bmatrix} 0.5 & 0 & 0 \\ 0 & 0.5 & 0 \\ 0 & 0 & 0.5 \end{bmatrix}$ $A_2 = \begin{bmatrix} -0.5 & 0 & 0 \\ 0.5 & -0.5 & 0 \\ 0 & 0 & -0.5 \end{bmatrix}$ $A_3 = \begin{bmatrix} 0.5 & 0 & 0 \\ 0 & 0.5 & 0 \\ 0.5 & 0 & 0.5 \end{bmatrix}$ | $\epsilon = \begin{bmatrix} 0.3 & 0 & 0 \\ 0 & 0.3 & 0 \\ 0 & 0 & 0.3 \end{bmatrix}$ |
| **Simulating Asymmetric Signal-to-noise (figure 3, 5A, 5B)** | |
| *Transfer Matrix* | *Noise Covariance Matrix* |
| $A_1 = \begin{bmatrix} 0.5 & 0 \\ 0 & 0.5 \end{bmatrix}$ $A_2 = \begin{bmatrix} -0.5 & 0.35 \\ 0.35 & -0.5 \end{bmatrix}$ $A_3 = \begin{bmatrix} 0.5 & 0 \\ 0 & 0.5 \end{bmatrix}$ | $\epsilon = \begin{bmatrix} 0.3 & 0 \\ 0 & 0.3 \end{bmatrix}$ |
| **Simulating Incomplete Signals for Conditioning: Serial (figure 8A, D)** | |
| *Transfer Matrix* | *Noise Covariance Matrix* |
| $A_1 = \begin{bmatrix} 0.5 & 0 & 0 \\ 0 & 0.5 & 0 \\ 0 & 0 & 0.5 \end{bmatrix}$ | $\epsilon = \begin{bmatrix} 0.3 & 0 & 0 \\ 0 & 0.3 & 0 \\ 0 & 0 & 0.3 \end{bmatrix}$ |

West et al. (2018): A Novel Non-Parametric Directionality Measure v5.3

Journal Pre-proof

$$A_2 = \begin{bmatrix} -0.5 & 0 & 0 \\ 0 & -0.5 & 0 \\ 0 & 0 & -0.5 \end{bmatrix}$$

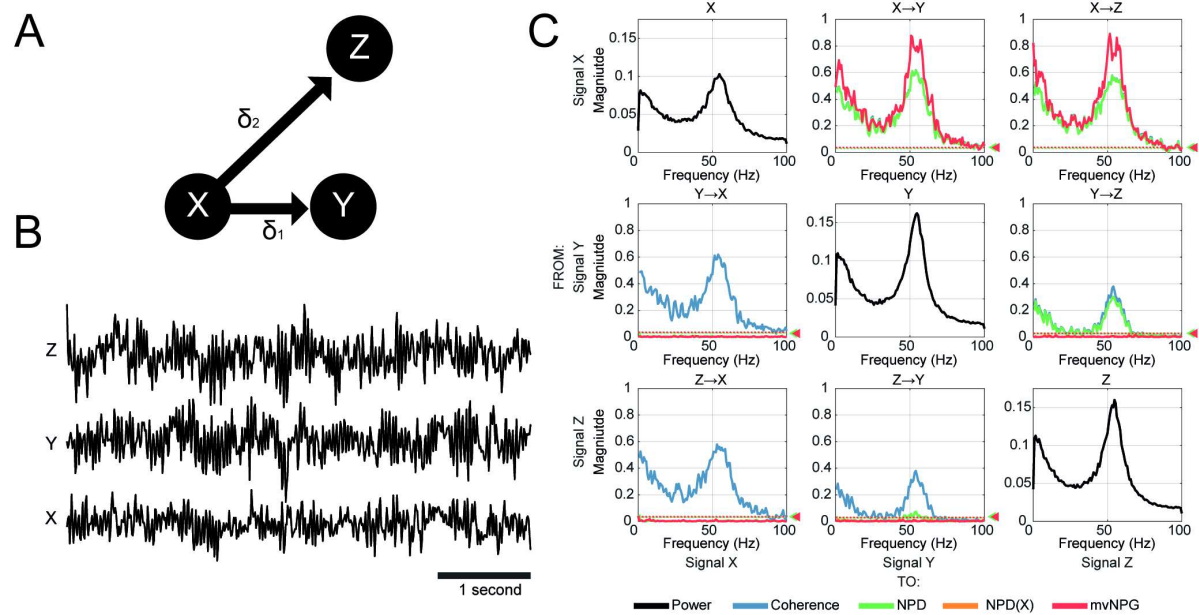$$A_3 = \begin{bmatrix} 0 & 0 & 0 \\ 0.3 & 0 & 0 \\ 0 & 0.3 & 0 \end{bmatrix}$$

**Simulating Incomplete Signals for Conditioning: Feedforward (figure 8B, E)**

| Transfer Matrix | Noise Covariance Matrix |
|---|---|

$$A_1 = \begin{bmatrix} 0.5 & 0 & 0 \\ 0 & 0.5 & 0 \\ 0 & 0 & 0.5 \end{bmatrix}$$

$$A_2 = \begin{bmatrix} -0.5 & 0 & 0 \\ 0 & -0.5 & 0 \\ 0 & 0 & -0.5 \end{bmatrix}$$

$$A_3 = \begin{bmatrix} 0.5 & 0 & 0 \\ 0 & 0.5 & 0 \\ 0.3 & 0 & 0.5 \end{bmatrix}$$

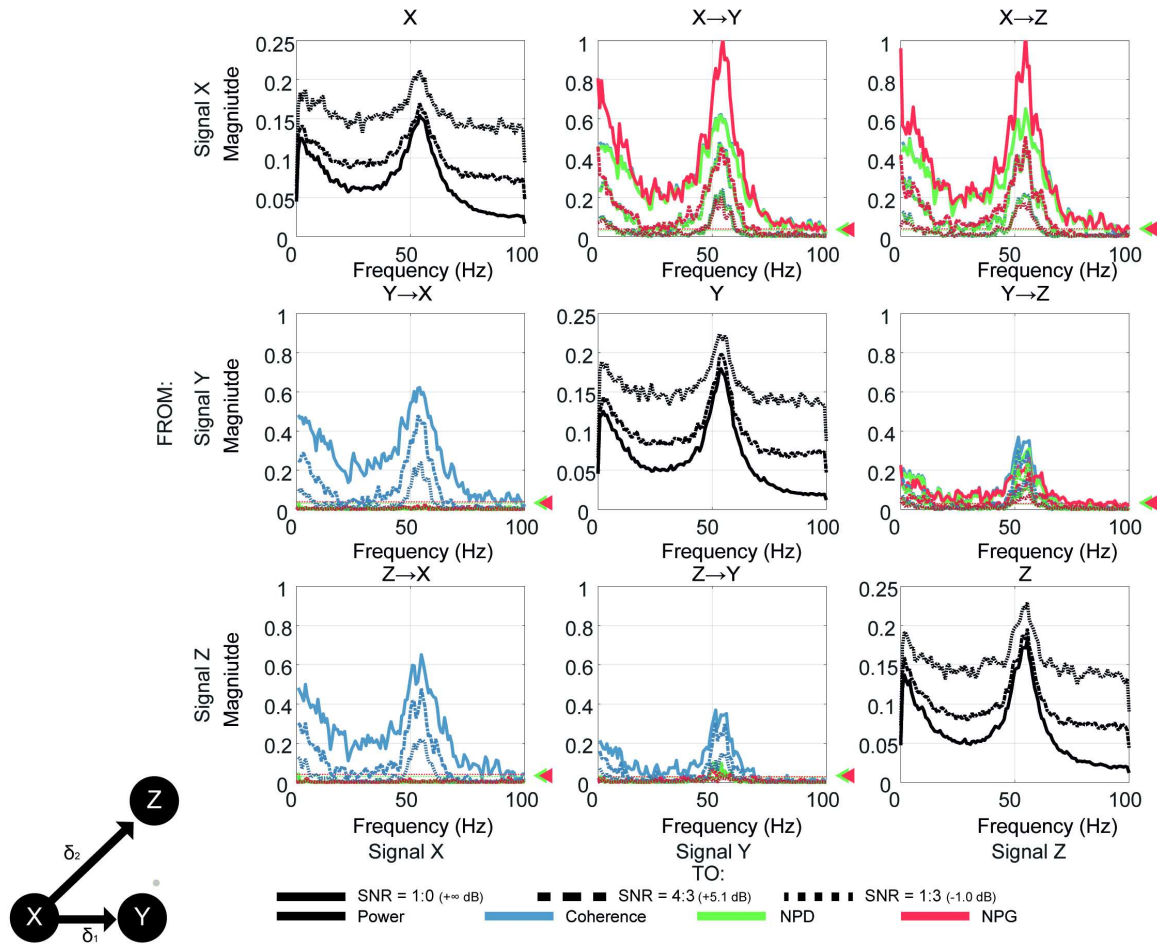$$\epsilon = \begin{bmatrix} 0.3 & 0 & 0 \\ 0 & 0.3 & 0 \\ 0 & 0 & 0.3 \end{bmatrix}$$

**Simulating Incomplete Signals for Conditioning: Recurrent (figure 68, F)**

| Transfer Matrix | Noise Covariance Matrix |
|---|---|

$$A_1 = \begin{bmatrix} 0.5 & 0 & 0 \\ 0 & 0.5 & 0 \\ 0 & 0 & 0.5 \end{bmatrix}$$

$$A_2 = \begin{bmatrix} -0.5 & 0 & 0 \\ 0 & -0.5 & 0 \\ 0 & 0 & -0.5 \end{bmatrix}$$

$$A_3 = \begin{bmatrix} 0 & 0.3 & 0 \\ 0 & 0 & 0.3 \\ 0.3 & 0 & 0 \end{bmatrix}$$

$$\epsilon = \begin{bmatrix} 0.3 & 0 & 0 \\ 0 & 0.3 & 0 \\ 0 & 0 & 0.3 \end{bmatrix}$$

1241

## 10.3 Permutation Testing for Significance Thresholds
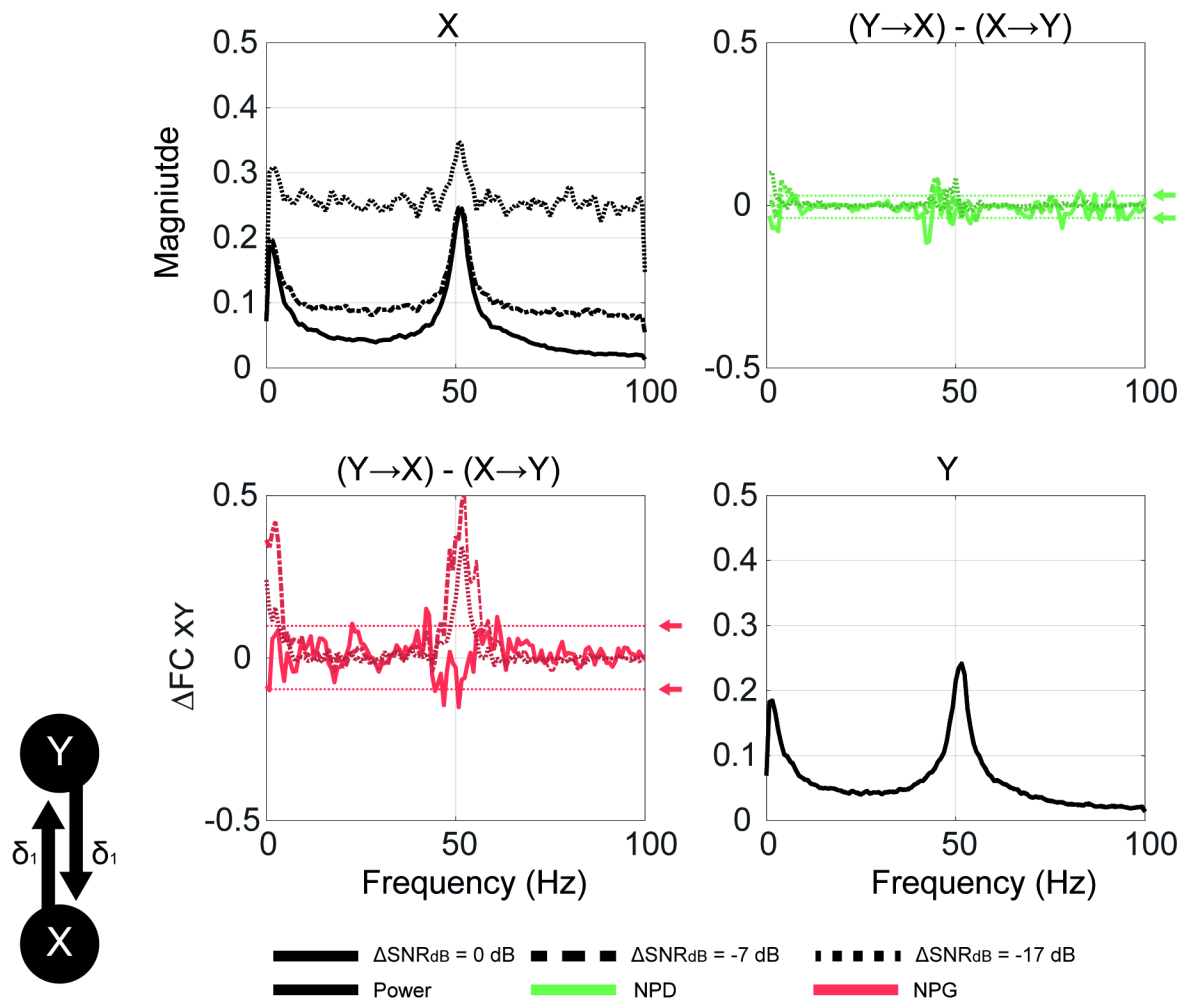
1242

1243 Estimates of interactions between signals can give rise to non-zero values in the absence of any
1244 interaction. To check whether an observed value of an estimator is statistically significant, its value
1245 can be compared against a distribution of the same index estimated from surrogate data (Theiler et al.
1246 1992). This surrogate data must preserve the statistics of the individual signals whilst removing the
1247 property to be tested, namely the interactions between them. Once a null distribution is obtained,
1248 (rank-order) significance thresholds can be calculated from the corresponding percentiles of the
1249 surrogate distribution (e.g. a $P = 0.01$ threshold can be estimated from the 99th percentile).

1250 Many possibilities exist for the generation of surrogates and methods range from the very simple
1251 permutation of the time series samples, up to increasingly complex surrogates that aim to maintain
1252 nonlinear features of the individual signals (for reviews see: Lancaster et al. 2018; Pereda et al. 2005).
1253 All methods will fall short at capturing all confounding properties of the individual generators of the
1254 signals including the phase randomization method (Zalesky and Breakspear 2015).
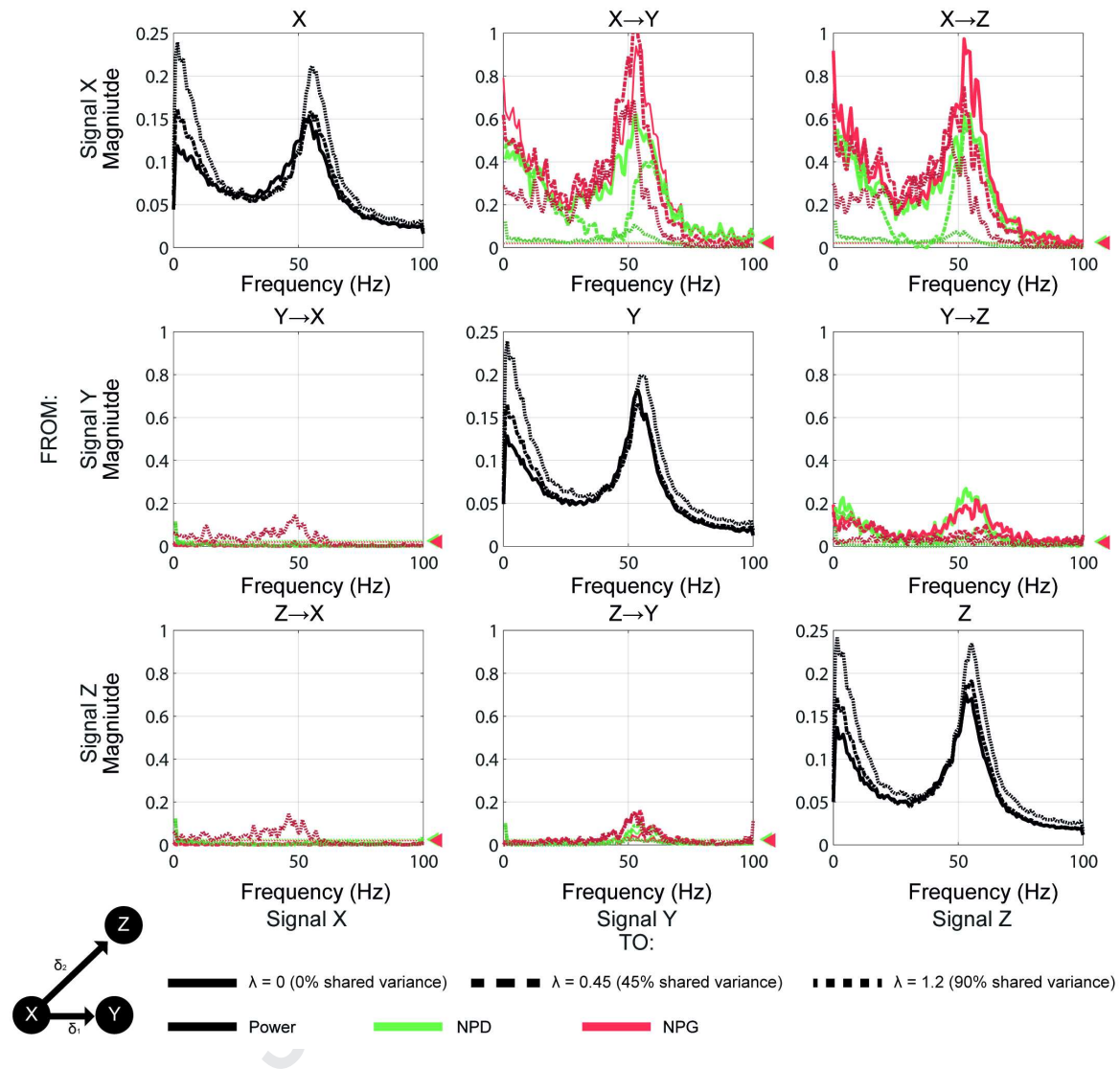
1255    In this work we use a phase randomization approach. We maintain the original FFTs of the signals but

1256    randomize the phase of the individual Fourier components. To do this we generate a vector of random

1257    phases $\Psi$ uniformly sampled on the interval $[0\ 2\pi]$ for N/2 samples and multiply the first half of the

1258    FFT by $\exp(i\Psi)$. The remainder of the FFT is then the horizontally flipped complex conjugate of the

1259    first half. This method ensures that the overall expected value of the magnitude of the averaged

1260    spectral estimate is equal to zero. See Lancaster et al. (2018) for a discussion of this method and

1261    Breakspear and Terry (2002) for application to assessing interdependence of neurophysiological
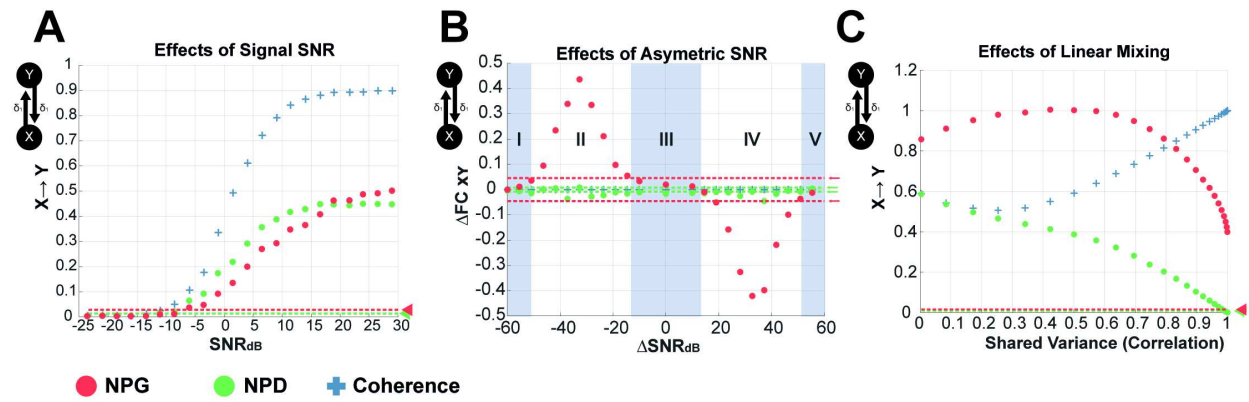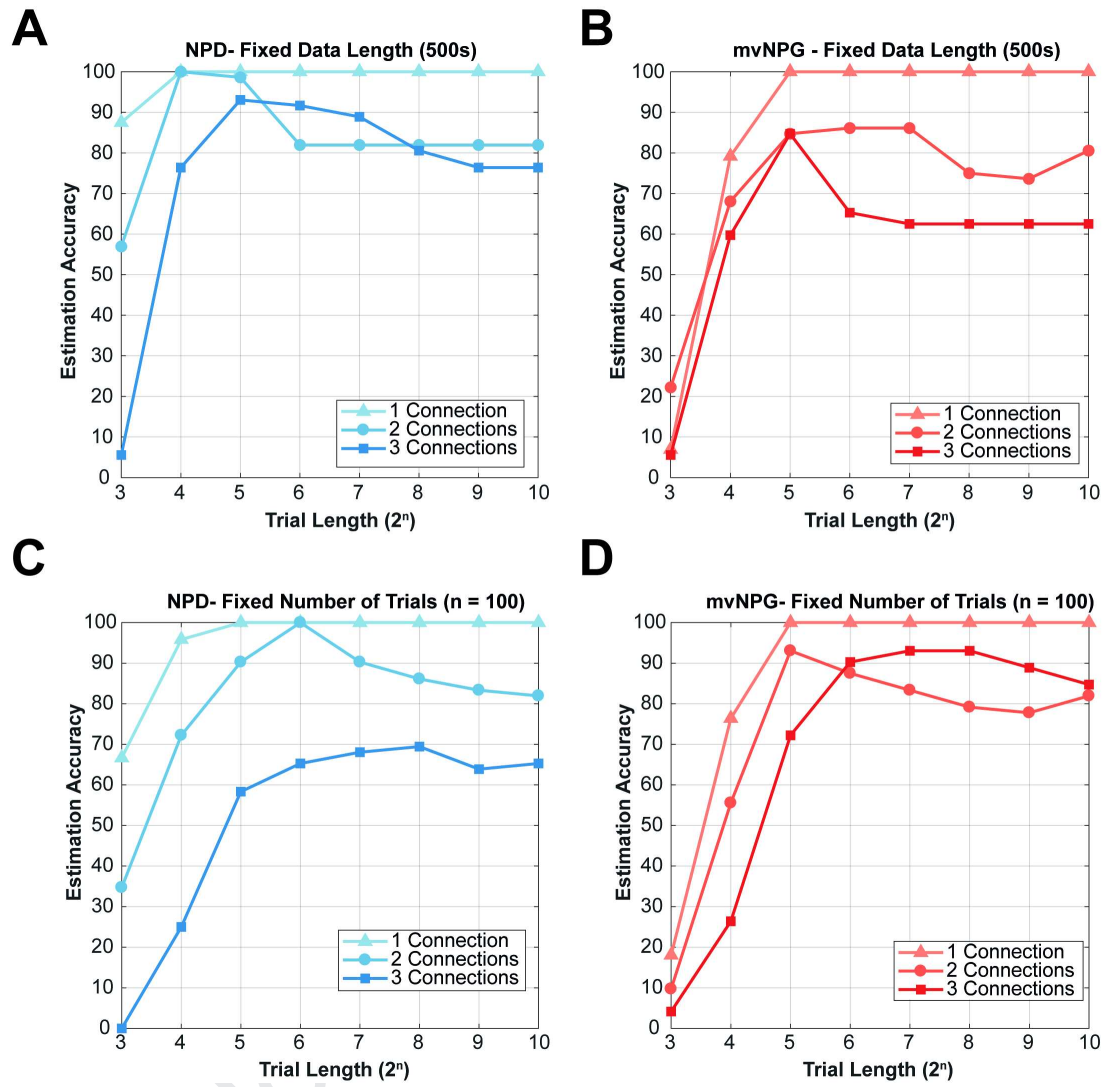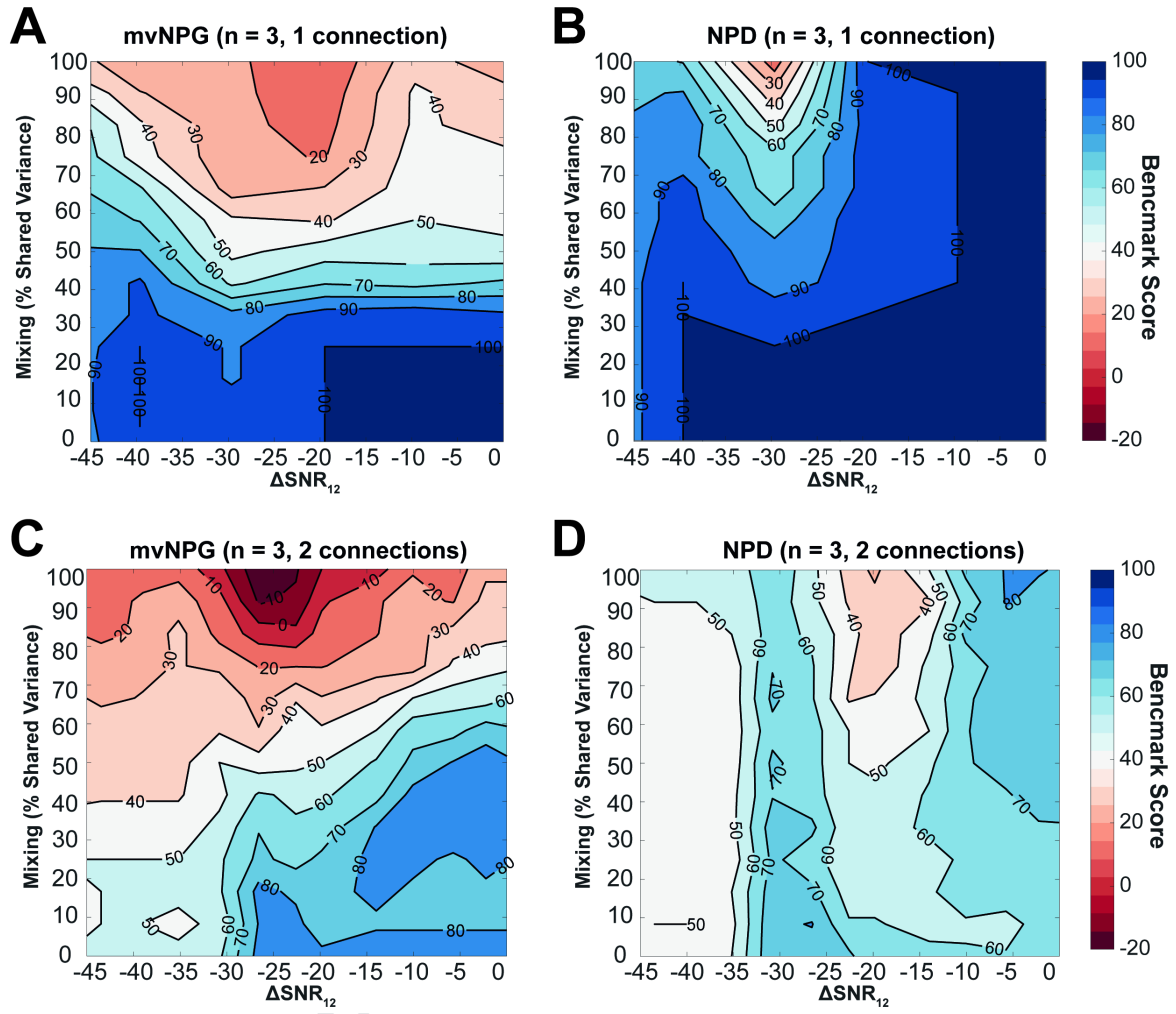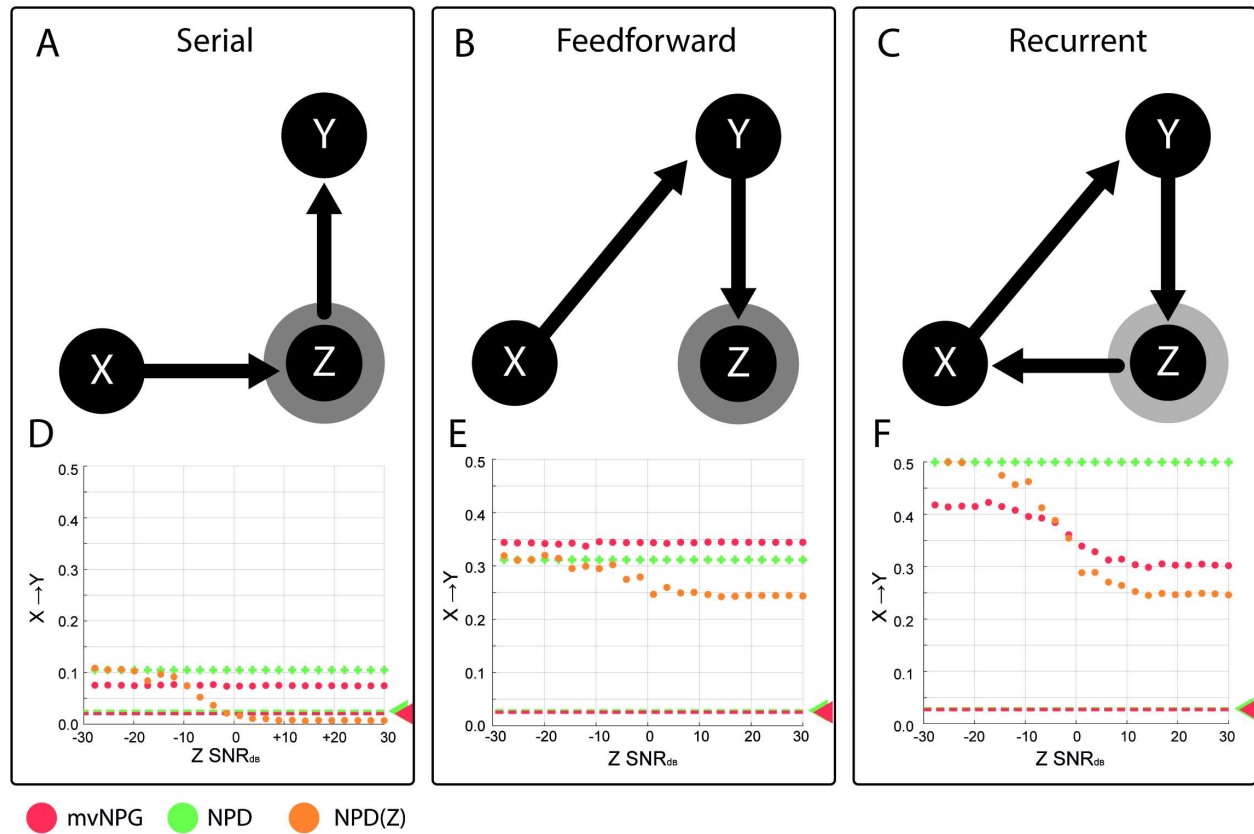
1262    signals.

**A** Effects of Signal SNR

**B** Effects of Asymetric SNR

**C** Effects of Linear Mixing

● NPG　● NPD　✚ Coherence

**A** NPD- Fixed Data Length (500s)

**B** mvNPG - Fixed Data Length (500s)

**C** NPD- Fixed Number of Trials (n = 100)

**D** mvNPG- Fixed Number of Trials (n = 100)

A Serial  B Feedforward  C Recurrent

D  E  F

mvNPG  NPD  NPD(Z)

## 1.1 Table of MVAR Coefficients

| **Simulating Common Drive, Signal-to-noise, instantaneous mixing (figure 1, 2, 4, 5C)** | |
|---|---|
| *Transfer Matrix* | *Noise Covariance Matrix* |
| $A_1 = \begin{bmatrix} 0.5 & 0 & 0 \\ 0 & 0.5 & 0 \\ 0 & 0 & 0.5 \end{bmatrix}$ $A_2 = \begin{bmatrix} -0.5 & 0 & 0 \\ 0.5 & -0.5 & 0 \\ 0 & 0 & -0.5 \end{bmatrix}$ $A_3 = \begin{bmatrix} 0.5 & 0 & 0 \\ 0 & 0.5 & 0 \\ 0.5 & 0 & 0.5 \end{bmatrix}$ | $\epsilon = \begin{bmatrix} 0.3 & 0 & 0 \\ 0 & 0.3 & 0 \\ 0 & 0 & 0.3 \end{bmatrix}$ |

| **Simulating (A)symmetric Signal-to-noise (figure 3, 5A, 5B)** | |
|---|---|
| *Transfer Matrix* | *Noise Covariance Matrix* |
| $A_1 = \begin{bmatrix} 0.5 & 0 \\ 0 & 0.5 \end{bmatrix}$ $A_2 = \begin{bmatrix} -0.5 & 0.35 \\ 0.35 & -0.5 \end{bmatrix}$ $A_3 = \begin{bmatrix} 0.5 & 0 \\ 0 & 0.5 \end{bmatrix}$ | $\epsilon = \begin{bmatrix} 0.3 & 0 \\ 0 & 0.3 \end{bmatrix}$ |

| **Simulating Incomplete Signals for Conditioning: Serial (figure 8A, D)** | |
|---|---|
| *Transfer Matrix* | *Noise Covariance Matrix* |
| $A_1 = \begin{bmatrix} 0.5 & 0 & 0 \\ 0 & 0.5 & 0 \\ 0 & 0 & 0.5 \end{bmatrix}$ $A_2 = \begin{bmatrix} -0.5 & 0 & 0 \\ 0 & -0.5 & 0 \\ 0 & 0 & -0.5 \end{bmatrix}$ $A_3 = \begin{bmatrix} 0 & 0 & 0 \\ 0.3 & 0 & 0 \\ 0 & 0.3 & 0 \end{bmatrix}$ | $\epsilon = \begin{bmatrix} 0.3 & 0 & 0 \\ 0 & 0.3 & 0 \\ 0 & 0 & 0.3 \end{bmatrix}$ |

| **Simulating Incomplete Signals for Conditioning: Feedforward (figure 8B, E)** | |
|---|---|
| *Transfer Matrix* | *Noise Covariance Matrix* |
| $A_1 = \begin{bmatrix} 0.5 & 0 & 0 \\ 0 & 0.5 & 0 \\ 0 & 0 & 0.5 \end{bmatrix}$ $A_2 = \begin{bmatrix} -0.5 & 0 & 0 \\ 0 & -0.5 & 0 \\ 0 & 0 & -0.5 \end{bmatrix}$ $A_3 = \begin{bmatrix} 0.5 & 0 & 0 \\ 0 & 0.5 & 0 \\ 0.3 & 0 & 0.5 \end{bmatrix}$ | $\epsilon = \begin{bmatrix} 0.3 & 0 & 0 \\ 0 & 0.3 & 0 \\ 0 & 0 & 0.3 \end{bmatrix}$ |

| **Simulating Incomplete Signals for Conditioning: Recurrent (figure 6C, F)** | |
|---|---|
| *Transfer Matrix* | *Noise Covariance Matrix* |

$$A_1 = \begin{bmatrix} 0.5 & 0 & 0 \\ 0 & 0.5 & 0 \\ 0 & 0 & 0.5 \end{bmatrix}$$

$$A_2 = \begin{bmatrix} -0.5 & 0 & 0 \\ 0 & -0.5 & 0 \\ 0 & 0 & -0.5 \end{bmatrix}$$

$$A_3 = \begin{bmatrix} 0 & 0.3 & 0 \\ 0 & 0 & 0.3 \\ 0.3 & 0 & 0 \end{bmatrix}$$

$$\epsilon = \begin{bmatrix} 0.3 & 0 & 0 \\ 0 & 0.3 & 0 \\ 0 & 0 & 0.3 \end{bmatrix}$$